

Deep phenotyping and lifetime trajectories reveal limited effects of longevity regulators on the aging process in C57BL/6J mice

Received: 25 March 2022

Accepted: 27 October 2022

Published online: 11 November 2022

 Check for updates

A list of authors and their affiliations appears at the end of the paper

Current concepts regarding the biology of aging are primarily based on studies aimed at identifying factors regulating lifespan. However, lifespan as a sole proxy measure for aging can be of limited value because it may be restricted by specific pathologies. Here, we employ large-scale phenotyping to analyze hundreds of markers in aging male C57BL/6J mice. For each phenotype, we establish lifetime profiles to determine when age-dependent change is first detectable relative to the young adult baseline. We examine key lifespan regulators (putative anti-aging interventions; PAAs) for a possible countering of aging. Importantly, unlike most previous studies, we include in our study design young treated groups of animals, subjected to PAAs prior to the onset of detectable age-dependent phenotypic change. Many PAA effects influence phenotypes long before the onset of detectable age-dependent change, but, importantly, do not alter the rate of phenotypic change. Hence, these PAAs have limited effects on aging.

A large body of work, carried out over the past decades in a range of model organisms including yeast, worms, flies and mice, has identified hundreds of genetic variants as well as numerous dietary factors, pharmacological treatments and other environmental variables that can increase the length of life in animals^{1–3}. Current concepts regarding the biology of aging⁴ are in large part based on results from these lifespan studies. Much fewer data, however, are available to address the question of whether these factors, besides extending lifespan, in fact also slow aging, particularly in the context of mammalian models.

It is important to distinguish lifespan vs. aging because it is well known that lifespan can be restricted by specific sets of pathologies associated with old age, rather than being directly limited by a general decline in physiological systems. In various rodent species, for instance, the natural end of life is frequently due to the development of lethal neoplastic disorders: Cancers have been shown to account for ca. 70–90% of natural age-related deaths in a range of mouse strains^{5–10}. Accordingly, there is a strong need to study aging more directly, rather than to rely on lifespan as the sole proxy measure for aging.

‘Aging’ is used as a term to lump together the processes that transform young adult individuals (i.e., individuals that have attained

full growth and maturity) into aged ones with functional changes across multiple physiological systems, elevated risk for multiple age-related diseases, and high mortality rates^{3,11,12}. It is associated with the accumulation of a large number of phenotypic changes, spanning across various levels of biological complexity (molecular, cellular, tissue and organismal level) and affecting virtually all tissues and organ systems^{13,14}. Aging can hence be approached analytically by assessing age-dependent phenotypic change, from young adulthood into old age, across a large number of age-sensitive traits covering multiple tissues, organ systems and levels of biological complexity^{15,16}.

Deep phenotyping represents a powerful approach to capture a wide range of aging-associated phenotypic changes, since it takes into account alterations at molecular, cellular, physiological and pathological levels of analysis, thereby providing a very fine-grained view of the consequences of aging as they develop across tissues and organs^{10,15–17}. The approach is therefore ideally suited to assess genetic variants, pathways, dietary or pharmacological factors previously linked to lifespan extension and, potentially, delayed aging. Deep phenotyping examines hundreds of parameters, many of which are expected to differ between young and old animals (hereafter called age-sensitive phenotypes; ASPs); these can be collectively used to

 e-mail: Dan.Ehninger@dzne.de

address if and how a given intervention interacts with the biological processes underlying the signs and symptoms of aging (Fig. 1a).

We here refer to the mechanisms of aging as the sets of processes that underlie age-dependent phenotypic change^{3,11,12}. Accordingly, an intervention that targets the mechanisms underlying aging should slow the transformation of a phenotypically

young to a phenotypically aged organism. In other words, the intervention should attenuate the age-dependent change in ASPs (the delta in phenotype between young and old). For instance, a specific intervention or genotype could ameliorate the age-dependent loss of neurons by promoting processes concerned with maintaining the integrity of neurons over time.

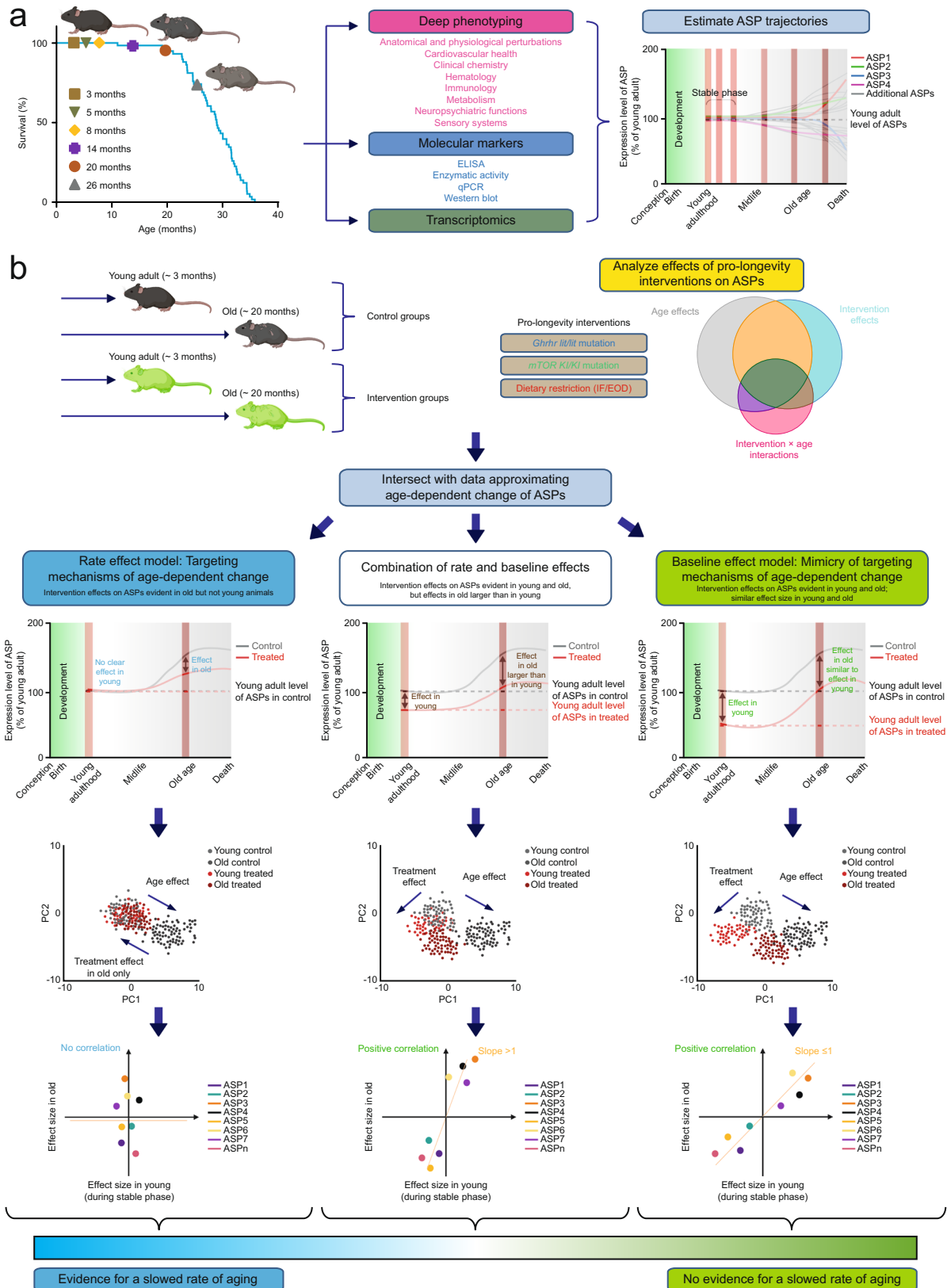


Fig. 1 | To what extent can aging, measured as a multidimensional representation of age-dependent phenotypic change, be slowed in mice? **a** To estimate aging trajectories for a wide range of age-sensitive phenotypes (ASPs), we examined phenotypes across the lifespan of C57BL/6J mice, including hundreds of phenotypes derived from multi-dimensional deep phenotyping, a range of molecular markers as well as transcriptomic profiles. **b** We assessed three important pro-longevity interventions for their effects on aging (putative anti-aging interventions; PAAIs). For each PAAI, we generated a young as well as an old cohort of experimental animals and controls, all of which were analyzed concurrently in one single study. For each phenotype in each of these studies, we determined age effects, intervention effects and intervention \times age interactions based on the data derived from young and old control as well as experimental animals. These analyses revealed that some ASPs were influenced (countered or accentuated) by the PAAIs, others not. For ASPs countered by PAAIs, we considered the following scenarios:

An intervention could mimic a targeting of age-dependent change by affecting ASPs directly (i.e., independently of age-dependent change in these phenotypes). For instance, a specific genetic variant may increase the number of neurons by promoting neurogenesis during brain development, without affecting the rate of subsequent age-dependent neuron loss. This variant would regulate neurodevelopmental processes but would not affect the mechanisms underlying age-dependent change. Although this would also result in increased neuronal numbers in old age, it cannot be taken as evidence of a slowed progression of aging because the rate of age-dependent change remains unaltered^{18,19}. Such a mimicry of effects on age-dependent change can be uncovered by dissociating the intervention's effects on ASPs from age-dependent changes in ASPs. Experimentally, this can be achieved by testing the intervention in young animals, prior to the onset of age-dependent change in ASPs.

These considerations are similar to the distinction between disease-modifying vs. symptomatic treatments made in clinical medicine^{20–23}. While both can be useful for patients, the former approach implies targeting the root causes of disease, whereas the latter does not. For instance, while a drug that enhances cognitive function in healthy people could serve well as a symptomatic treatment for subjects affected by Alzheimer's disease (AD), it does not provide clues regarding the mechanisms underlying cognitive decline in AD. Likewise, a drug that enhances cognitive function in pre-symptomatic AD patients, well before the onset of cognitive decline, is not lending insights into the mechanisms underlying AD-related cognitive decline because that's not what it is targeting. Clues regarding underlying pathogenetic processes can, however, be derived from a disease-modifying treatment that changes the rate of cognitive decline in AD.

Building on the considerations above, it is relatively straightforward to design experiments that distinguish between an intervention targeting age-dependent change and a mimicry of such an effect (Fig. 1; detailed analysis workflow is illustrated in Supplementary Fig. 1). One needs to 1) generate knowledge of lifetime profiles of ASPs in order to determine when age-dependent changes in ASPs are first detectable (Fig. 1a) to then 2) design experiments that include young treated reference groups, which are subjected to a putative anti-aging intervention (PAAI) prior to age-dependent changes in ASPs (Fig. 1b).

Based on these fundamental considerations, we sought to estimate aging trajectories for a compendium of ASPs. Towards this end, we profiled hundreds of phenotypes, and thousands of molecular markers, across the lifespan of mice; these analyses included multi-dimensional deep phenotyping, assessments of a range of molecular markers as well as transcriptomic profiling and were carried out in 3, 5, 8, 14, 20 and 26 month old male C57BL/6J mice (Fig. 1a). We hypothesized that individual ASPs follow different lifetime trajectories and that for many ASPs there is an initial stage of relative stability in young adulthood, with limited changes in many of the parameters examined (Fig. 1a, see schematic to the right). If this were correct, young groups

PAAIs could influence ASPs in a way consistent with slowing the rate of age-dependent change in ASPs (rate effect), via age-independent effects on ASPs (baseline effect) or via a combination of rate and baseline effects. To address what the age at first detectable change is for each ASP influenced by an intervention, we intersected data on ASPs from these intervention studies (see panel **b**) with data from our baseline study (see panel **a**). We compared effect sizes to examine for each ASP individually whether PAAI effects differed measurably between young and old mice. In addition, we used dimensionality reduction approaches as well as intraclass correlation analyses of intervention effect sizes in young and old animals to determine whether PAAIs overall act on ASPs primarily in a way consistent with slowing their rate of age-dependent change (left panels), via age-independent effects (right panels) or via a combination of rate and baseline effects (middle panels). For further details on our analytical approach, see Supplementary Fig. 1. Created with BioRender.com.

(younger than the age at first detected age-dependent change in many ASPs) could be used to determine whether a PAAI interacts with age-dependent changes by either modifying their root causes or by acting on ASPs in an age-independent manner. Consistent with our hypothesis, we demonstrate that most of the phenotypes examined in this study feature a period of relative stability in young adulthood (i.e., between 3 and 5 months of age).

We then applied the strategy outlined above to assess key longevity interventions in animal models for their effects on aging (slowing aging rate vs. age-independent effects). Major insights into longevity-associated pathways have predominantly derived from lifespan studies of genetically modified organisms^{1,3}. mTOR signaling and growth hormone signaling are amongst the most central regulators of lifespan according to prior longevity studies in *C. elegans*, *D. melanogaster* and mice^{9,16,24–55}. The mTOR pathway also represents a major focus of efforts to develop pro-longevity drugs (e.g. ref. 56). Accordingly, to cover key genetic longevity interventions and study their effects on aging in mice, we here chose genetic models targeting the mTOR pathway (hypomorphic *mTOR^{KI/KI}* mice^{35,57,58}) as well as growth hormone signaling (*Ghrh^{lit/lit}* mice^{59,60}). In parallel to our studies in mice, we applied multi-dimensional phenotyping combined with stratification based on genetic expression variants in *GHRHR* and *MTOR* in a human population across a wide age range, spanning from 30 to 95 years⁶¹. The analyses in humans complement our work in animal models and allowed us to address, in parallel to the work in mice, whether or not a potential genetic modification of human ASPs occurs in an age-independent fashion or not.

In addition to these genetic factors, we applied our deep phenotyping strategy to assess an important environmental longevity intervention for its effects on aging (slowing aging rate vs. age-independent effects). Among the most intensely studied environmental factors are dietary restriction effects on longevity and age-related changes, with many thousands of publications since the 1930s when the effects of food restriction on lifespan in rodents were first discovered⁶². Accordingly, in our study, we chose to examine a dietary restriction model (specifically, a form of intermittent fasting/every other day feeding) that has been previously linked to lifespan extension in mice^{10,63}.

Finally, we integrated our aging trajectory dataset with the analyses of PAAIs to address whether PAAIs primarily counteracted signs of aging in ways consistent with a slowing of age-dependent changes in ASPs (Fig. 1b, panels to the lower left; rate effects) or via a mimicry of such effects (Fig. 1b, panels to the lower right; baseline effects).

PAAIs can also affect ASPs via a mixture of baseline and rate effects (Fig. 1b, panels in the lower middle). This pattern corresponds to having effects in both age groups with effects being larger in old mice than in young mice. One possible interpretation of such a pattern is that PAAIs could have age-independent effects in addition to slowing aging-associated change in phenotype. Alternatively, this constellation of findings could be caused simply by differences in treatment

exposure time between young (shorter-term exposure leading to weaker effects) and old animals (longer exposure leading to stronger effects). Our current study design does not allow us to distinguish between these two possible interpretations. Hence, this intermediate category (Fig. 1b, panels in the lower middle) identifies ASPs with candidate status for a slowed rate of age-dependent change which, however, requires further study and corroboration.

Our current analyses reveal that, among all PAAIs examined, many “anti-aging” effects are age-independent in nature (i.e., interventions have similar effect sizes in young and old mice), suggesting these phenotypes are not affected by a deceleration of age-dependent change. We also identify phenotypes influenced by PAAIs in a way consistent with a slowed aging rate, although these reflect a minority of ASPs analyzed. Our findings have important implications regarding the extent to which different aspects of the aging process can be modulated, at least by the set of PAAIs investigated in the present study.

Results

Age-dependent phenotypic change in our older groups of mice

To map age-dependent trajectories of a broad range of phenotypes over the lifespan of mice, we carried out deep phenotyping analyses in 3, 5, 8, 14, 20 and 26 month old male C57BL/6J mice. This covered phenotypes within the areas of cardiovascular health, neuropsychiatric functions, sensory systems, clinical chemistry, hematology, immunology, metabolism, as well as anatomy and physiology (for details regarding the assays used and phenotypes analyzed, see Supplementary Table 1, Supplementary Data 1, 2 and the Methods section; for details regarding pathological findings in this cohort of animals, see Supplementary Fig. 2) (Fig. 2a).

Overall, this analysis included 222 phenotypes, ~59% of which we found to be age-sensitive ($p < 0.05$ by one-way ANOVA with between-subjects factor age, Kruskal–Wallis-test or Fisher’s exact test, as appropriate). ASPs were observed across all functional domains examined (Fig. 2b). Based on the outcomes of posthoc analyses relative to the young reference group (3 months old group; for details, see Material and Methods), we next assigned ASPs into any one of the following categories: ASPs first detectable at either 5, 8, 14, 20 or 26 months, or others (Fig. 2c, d).

Only ~5% of ASPs featured very early alterations, with an age at first detected change of 5 months; a progressively diminishing acoustic startle response, indicative of early-onset age-related hearing loss associated with a degeneration of cochlear hair cells and spiral ganglion neurons in C57BL/6J mice⁶⁴, represents an example in this category (Fig. 2e). We also noted very few ASPs with an age at first detected change of 8 months (~5% of all ASPs). For instance, the abundance of naïve CD4⁺ T cells (CD62L⁺CD4⁺ T cells), which is well known to decline with advancing age^{16,65–67} and is linked to age-related impairments in adaptive immune responses^{65–67}, started to show measurable decrements at 8 months and continued to decrease further in the older age groups (Fig. 2e).

We noted that ~26% of ASPs showed a difference first measurable at 14 months. An increased duration of the QRS interval, a well-known electrocardiographic aging phenotype in mice^{10,68} and men⁶⁹ that might reflect slowed ventricular depolarization due to altered intercellular communication between cardiomyocytes⁶⁸, serves as an example to illustrate this pattern of age-related change (Fig. 2e).

Many ASPs (~36%) were characterized by changes that became detectable only later in life, with reliable alterations first identified at 20 months. The age-related reduction of exploratory activity in an unfamiliar environment (open field), for instance, constitutes a well-known ASP^{10,16,70} and was first observed in 20-month old mice (Fig. 2e). Finally, few changes (~8%) were first noted in 26-month old mice. Alterations in platelet morphology showed a detectable departure from baseline at 26 months (Fig. 2e). In addition to age-related

alterations showing a consistent direction of change once they had emerged, we also noted a subset of phenotypes with other lifetime profiles (~19%, denoted as ‘other’): Fat mass for instance first increased to a peak in midlife and then decremented in older age groups (Fig. 2e).

We carried out principal component analysis (PCA) to determine how the animals from all our age groups cluster in 2D-PCA space based on all phenotypes (measured on a continuous scale) included in the deep phenotyping analysis (Fig. 2f). Age effects were mostly seen in PC1. There was no apparent difference between 3-month and 5-month old animals on PC1. A PC1 shift to the right appeared to be first evident at 8 months and progressively increased up to 20 months.

In conclusion, our deep phenotyping analysis identified a large number of ASPs and showed only very limited age-related changes in these phenotypes between 3 and 5 months of age. The analyses also indicated that, overall, most changes in ASPs from baseline were detected in the second year of life of the animals (between 14 and 20 months).

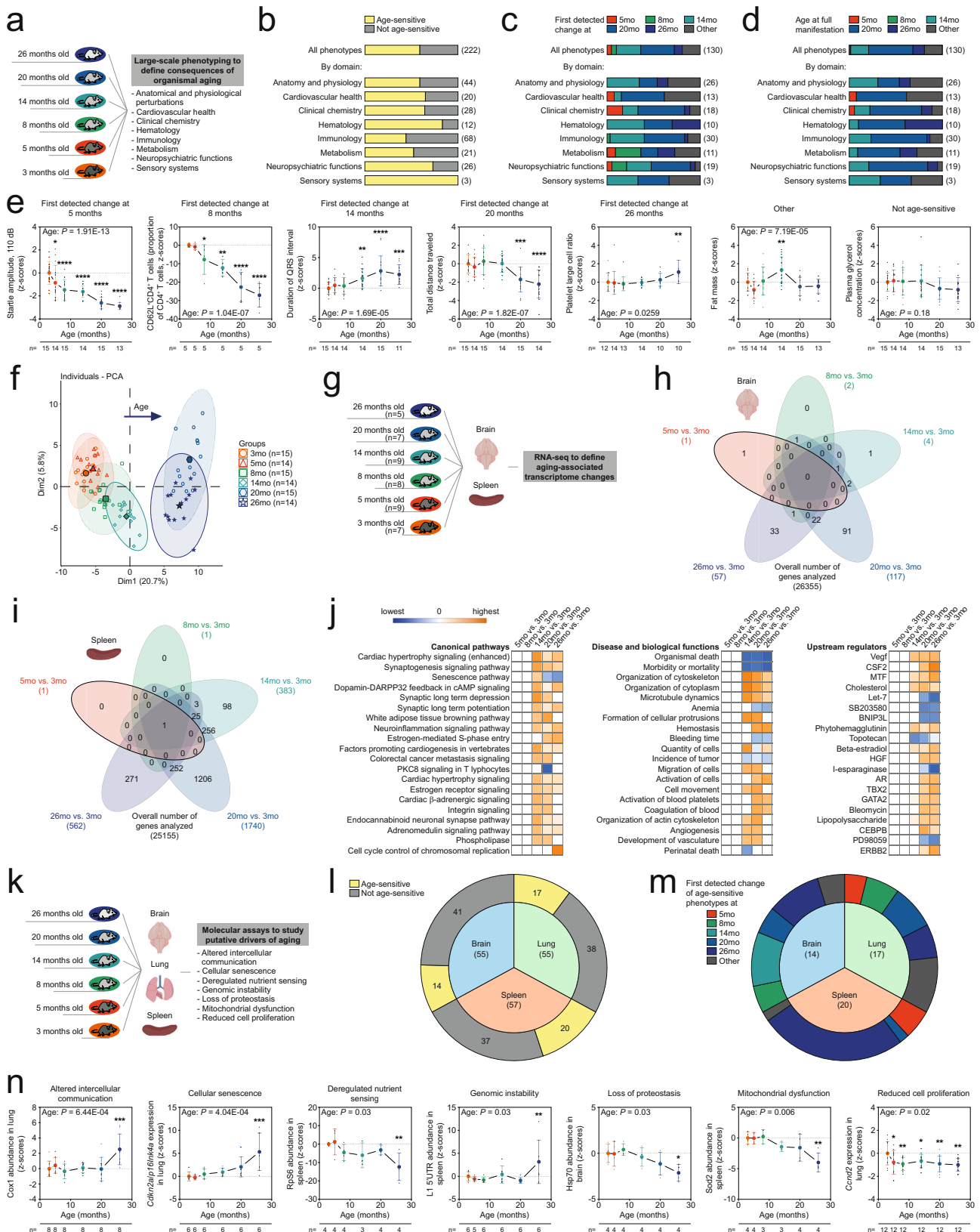
Next, we employed RNA-seq analyses to determine the age in life when transcriptomic changes relative to the young adult baseline are first discernable in our cohort of animals (Fig. 2g–j; Supplementary Fig. 3; Supplementary Data 3–5). As starting material, we used brain and spleen tissue, respectively, of 3, 5, 8, 14, 20 and 26 month old male C57BL/6J mice. Consistent with the data described above, we observed very limited changes in gene expression when comparing 3-month old mice to 5- or 8-month old animals for both brain and spleen tissue (Fig. 2h, i; Supplementary Fig. 3). While in spleen many changes relative to the young adult baseline began to be detectable at 14 months (Fig. 2i, j; Supplementary Data 3), significant differences relative to the 3-month baseline in brain were largely restricted to the two oldest groups (20 and 26 months; Fig. 2h; Supplementary Fig. 3; Supplementary Data 4).

To establish how molecular and cellular mechanisms that have been suggested to drive aging are altered across the murine lifespan⁴, we analyzed a panel of molecular markers that we designed to cover many hallmark processes of aging (summarized in Supplementary Tables 2–4; Supplementary Fig. 4). These included markers to assess alterations in intercellular communication, cellular senescence, deregulated nutrient sensing, genomic stability, loss of proteostasis, mitochondrial dysfunction and reduced cell proliferation (Fig. 2k). These analyses were focused on spleen, lung and brain of 3, 5, 8, 14, 20 and 26 month old male C57BL/6J mice. Based on the set of molecular markers tested, age-associated alterations were noted in 14 out of 55 in the brain, 17 out of 55 in the lung and 20 out of 57 in the spleen (Fig. 2l; Supplementary Data 6). Among all age-sensitive markers, most showed relative stability between 3 and 5 months and clear changes, compared to the young adult baseline (3 months), were detectable primarily in the oldest groups (20 and 26 months) (Fig. 2m; Supplementary Data 6). An exception to this notion were age-related changes in cell proliferation markers that decremented early (between 3 and 5 months) and remained stable afterwards (Fig. 2m, n; Supplementary Data 6). In summary, our analyses of molecular markers were consistent with the deep phenotyping data described above in showing relative stability in early life; most age-related changes relative to the young adult baseline were identified past the first year of life.

Altogether, the data discussed thus far, including deep phenotyping, molecular and transcriptomic data, revealed that few age-sensitive markers show alterations detectable early in life (between 3 and 5 months). Rather, most changes relative to the young adult baseline (3 months) detected in our study became apparent in the second year of life.

Do key longevity factors slow aging in mice?

We wanted to establish whether key longevity and putative anti-aging interventions (PAAIs), on a large scale, counter age-sensitive phenotypes (ASPs). We also wanted to address whether effects on ASPs are



best explained via (1) slowing the development of age-related changes in ASPs, (2) age-independent effects on ASPs or (3) a combination of (1) and (2). To explore which of these scenarios is supported best empirically, we analyzed deep phenotyping and transcriptomic effects of key longevity interventions. For each PAAI, we generated a young as well as an old cohort of experimental animals and controls, all of which

were analyzed concurrently. We chose the young group to be 3 months of age when the analyses commenced and ~5 months at their completion, implying that the measurements were carried out during a period of relative stability of most ASPs (Fig. 2; Supplementary Data 1, 2). Accordingly, effects on ASPs seen in the young groups should be largely interpreted as aging-independent effects. We chose the old

Fig. 2 | Multidimensional analyses of age-dependent phenotypic change in C57BL/6j mice. a–f Deep phenotyping results in wildtype C57BL/6j mice. **a** Schematic illustration of deep phenotyping study design. Mouse symbols adapted from ref. 10. **b** Relative proportion of ASPs among all phenotypes examined. Age at first detectable change (**c**) and age at full manifestation (**d**) of ASPs shown as proportion of all ASPs. **e** Representative examples of ASPs with various ages at first detectable phenotypic change. Data was analyzed using one-way ANOVA with the between-subjects factor age followed by Fisher's LSD posthoc analyses, where appropriate. **f** Principal component analysis of deep phenotyping data. **g–j** Summary of RNA-seq data. **g** Schematic illustration of RNA-seq study design. Venn diagram shows, for brain (**h**) and spleen (**i**), the number of differentially expressed genes (FDR < 0.05) relative to the 3-month old reference group together with the intersection of the corresponding gene sets. **j** Ingenuity Pathway Analysis shows top canonical pathways, diseases and biological functions as well as predicted upstream regulators of genes differentially expressed in spleen relative to the 3-month old group. Positive z-scores (orange) indicate activating effects,

negative z-scores (blue) indicate inhibitory effects on corresponding processes. Pathway analyses of brain data are shown in Supplementary Fig. 3. **k–n** Summary of molecular analyses designed to study putative driver mechanisms of aging in spleen, lung and brain. **k** Schematic illustration of study design (for sample size, see Supplementary Data 6). **l** Proportion of age-sensitive molecular parameters obtained. **m** Proportion of the different age-at-first-detectable-change categories among all age-sensitive molecular markers in individual tissues. **n** Representative examples of molecular markers covering the different hallmarks of aging. Line plots (**e, n**) show means \pm S.D. (individual data points are superimposed; we did not use jittering to separate data points with identical values). Data was analyzed using one-way ANOVA with the between-subjects factor age followed by Fisher's LSD posthoc analyses, where appropriate. * $p < 0.05$, ** $p < 0.01$, *** $p < 0.001$, **** $p < 0.0001$ relative to 3-month young adult reference group. Sample sizes in each group and experiment are provided within the figure. Source data are provided in Source Data file. Created with BioRender.com.

groups to be ~20 months of age when the analyses started (completion at ~22 months) because the animals were old enough to have accumulated clear changes in ASPs but were still at an age before the steep increase in age-related mortality (Fig. 1a). This design choice was made to minimize confounding effects of differential survival in our analysis of mutant mice vs. controls.

A loss-of-function *Ghrhr* mutation attenuated ASPs often via age-independent mechanisms

We focused our analyses on two single-gene mutants, both associated with extension of lifespan in mice^{35,57,60} and each affecting a pathway generally considered to be pivotal in regulating lifespan and aging^{9,16,24–55,70–74}. First, we analyzed a mouse line with a loss-of-function mutation in *Ghrhr* (coding for the growth hormone releasing hormone receptor)⁵⁹ (Fig. 3; Supplementary Figs. 5, 6; Supplementary Data 7, 8). These *Ghrhr*^{lit/lit} mutant mice display deficiencies in growth hormone signaling, a dwarf phenotype, extension of lifespan and an amelioration of several age-sensitive phenotypes when analyzed in old age⁶⁰.

PCA of the deep phenotyping dataset we generated for the *Ghrhr*^{lit/lit} mutant line indicated similar genotype effects in the young and aged group of animals (see PC1 and PC2 in Fig. 3b). Based on axis contributions, the effect of genotype was about twice as large as the effect of age. Age effects on the first two principal components were similar in WT and *Ghrhr*^{lit/lit} mutants (Fig. 3b) with no clear evidence for an interaction of age and genotype.

Analyses of individual phenotypes (based on two-way ANOVA or aligned rank transform; for details, see also Material and Methods) revealed that, out of 206 phenotypes examined, 96 showed a significant main effect of age, 90 showed a significant main effect of genotype and 30 showed a significant interaction between genotype and age (Fig. 3c). Out of the 96 age-sensitive phenotypes, 35 were not significantly affected by genotype, 45 showed a significant main effect of genotype (but no interaction) and 16 featured a significant genotype \times age interaction (Fig. 3c). Further analyses of ASPs based on the results of posthoc tests are described in Supplementary Results, Supplementary Fig. 7 and Supplementary Data 8. Figure 4a–c shows standardized coefficients (with their 95% confidence intervals), corresponding to age effects, genotype effects and genotype \times age interactions, derived from linear models applied to all continuously distributed phenotypes included in the study. These analyses confirmed that most of the genotype influences are due to main effects of genotype and not genotype \times age interactions.

To assess whether genotype effects countered age effects or whether genotype and age effects influenced a phenotype in the same direction, we compared for each phenotype the directionality of Cohen's d effect sizes of age with those of Cohen's d effect sizes of genotype in the old group of mice. These analyses revealed that out of the set of 96 age-sensitive phenotypes 18 were further accentuated

by the *Ghrhr*^{lit/lit} genotype, while 38 were opposed by the *Ghrhr*^{lit/lit} genotype (Fig. 3c; Supplementary Data 7, 8; 5 ASPs could not be evaluated because Cohen's d effect sizes could not be computed due to 0 values in the denominator). Most of the 38 ASPs counteracted by *Ghrhr*^{lit/lit} genotype showed a significant main effect of genotype, but no significant interaction between genotype and age (Fig. 3c). Closer inspection of the ASPs featuring a significant interaction term (considering the directionality of change) indicated that ca. 10.4% of all ASPs identified correspond to ASPs counteracted by *Ghrhr*^{lit/lit} in ways consistent with the "rate effect model" or "combined rate/baseline effect model" introduced in Fig. 1b. Based on a significant genotype main effect, but a lack of an interaction, ca. 29.2% corresponded to ASPs consistent with the "baseline effect model" shown in Fig. 1b. The remaining ASPs were not affected (ca. 36.5%), accentuated (ca. 18.8%) by *Ghrhr*^{lit/lit} or could not be evaluated (ca. 5.2%). All the *Ghrhr*^{lit/lit}-opposed ASPs we were able to evaluate had an age at first detectable departure from young adult baseline of 8 months (Fig. 3c); hence, all the corresponding genotype effects on ASPs in young animals appear independent of age-related change in those ASPs (since age-dependent changes in ASPs have not yet manifested in young animals).

To examine further the relationships between age and genotype effects, we performed correlation analyses comparing the Cohen's d effect sizes of age vs. the *Ghrhr*^{lit/lit} genotype. We found a modest inverse relationship between age effects and genotype effects in old mice (Fig. 3d). We noted a similar inverse relationship when regressing the effect size of age with the effect size of the *Ghrhr*^{lit/lit} mutation in the young cohort of animals (Fig. 3e).

We next asked whether genotype effects are similar across age groups within the category of ASPs countered in *Ghrhr*^{lit/lit} mutants ($n = 38$ phenotypes). Towards this end, we performed linear regression analyses of genotype effects in the young vs. the old group of mice for these $n = 38$ phenotypes. For all ASPs countered by the *Ghrhr*^{lit/lit} genotype, these analyses revealed an overall high similarity of genotype effects across age groups (Fig. 3g; $R = 0.83$, $p = 1.53E-10$), indicating that homozygosity for the *Ghrhr*^{lit} mutant allele resulted in similar phenotypic consequences on ASPs irrespective of the age of the animal. The slope of the regression line was 0.91 ± 0.1 (95% CI: 0.70, 1.12; $p = 0.3975$), thereby supporting the notion of overall similar effect sizes in young and old mice in this category of genotype-sensitive ASPs (Fig. 3g; 1 corresponding to the same effect sizes in young and old; values significantly <1 to effect sizes overall larger in young mice; values significantly >1 to effect sizes overall larger in old mice). Similar results were obtained using intraclass correlation analyses (Fig. 3g; ICC = 0.83, $p = 1.88E-11$) which reflect not only the degree of correlation but also the agreement between measures in the young and old group. For instance, consistent with prior research^{16,75}, advancing age led to an increased latency to respond on the hot plate test, indicative of aging-associated alterations in nociceptive function, and the *Ghrhr*^{lit}

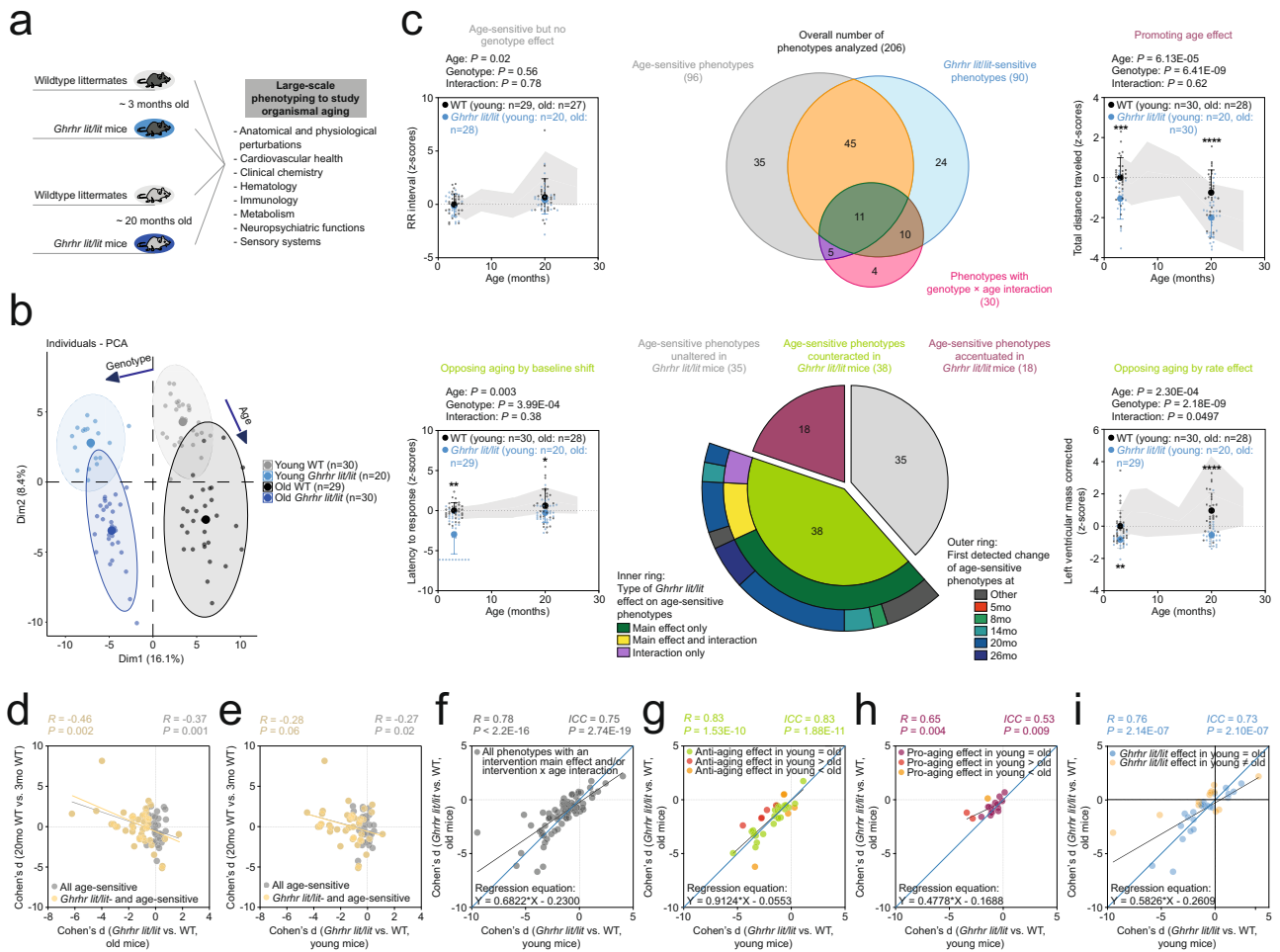


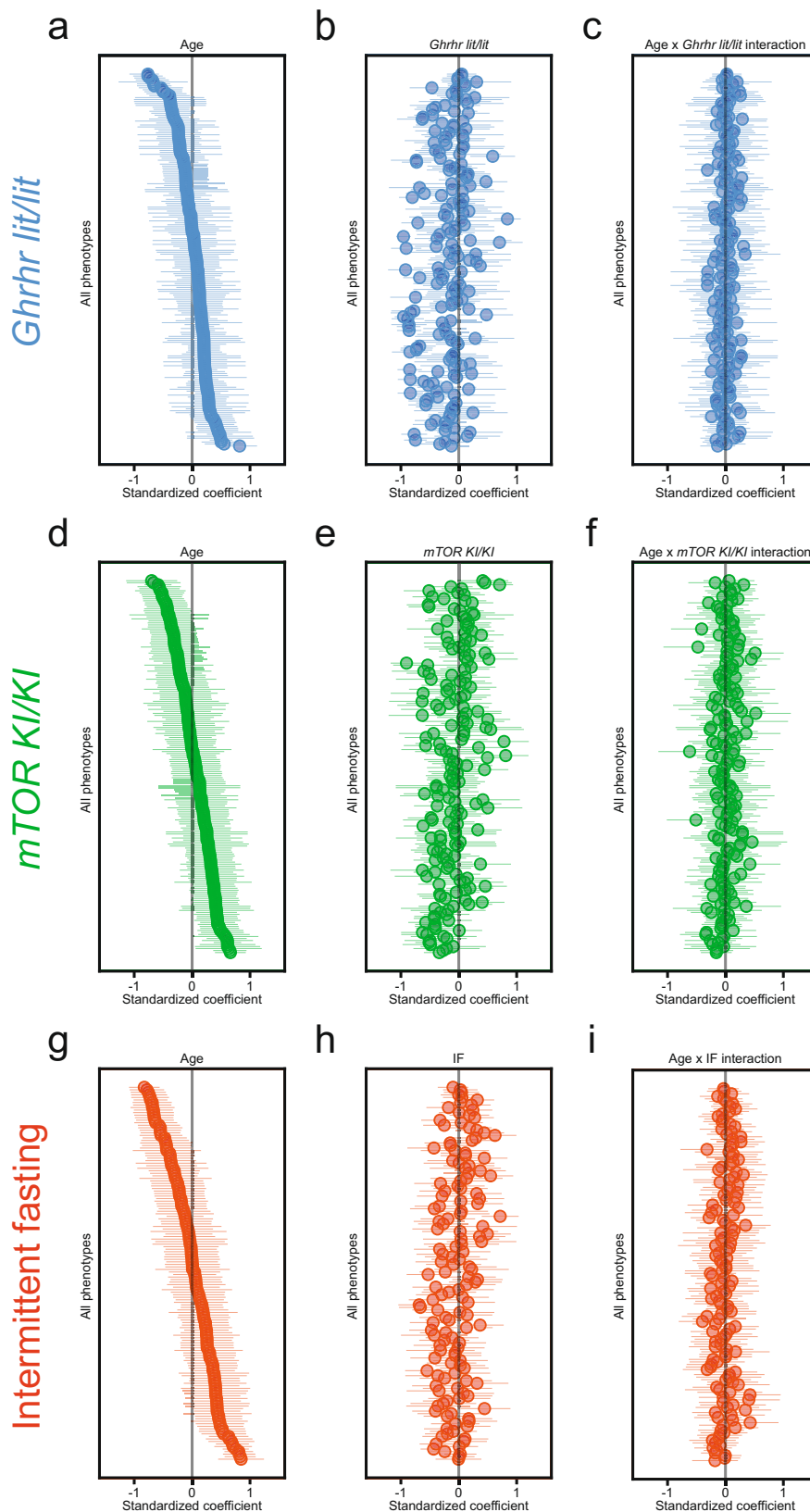
Fig. 3 | ‘Anti-aging’ effects induced by the *Ghrhr*^{fl/fl} mutation manifested mostly in young mice (prior to detectable age-dependent phenotypic changes). **a–i** Deep phenotyping results in *Ghrhr*^{fl/fl} mice. **a** Schematic illustration of study design. Mouse symbols adapted from ref. 10. **b** Principal component analysis of deep phenotyping data. **c** Venn diagram shows the number of ASPs, genotype-sensitive phenotypes, phenotypes with a genotype × age interaction and their intersection. Sunburst chart shows the number of ASPs either unaltered, counteracted or accentuated by genotype. For ASPs counteracted by genotype, the inner ring shows the proportion of phenotypes with either a genotype main effect, a genotype × age interaction or both. The outer ring shows when changes in the corresponding ASPs were first detected in our baseline study. Line charts show representative examples of phenotypes influenced by age and/or intervention in the different possible ways. Data are presented as z-scores (normalized to the young WT group) and are plotted as mean ± S.D. (individual data points are superimposed). Two-way ANOVAs with the between-subjects factors age and

genotype followed by Fisher’s LSD posthoc analyses, where appropriate, were used for data analysis. * $p < 0.05$, ** $p < 0.01$, *** $p < 0.001$ relative to age-matched wildtype littermate controls. Life-time trajectories of the corresponding phenotypes, representing measurements obtained in our baseline study, are shown by the gray-shaded area in the background (bounded by mean ± S.D.). Effect size of genotype in old (**d**) or young (**e**) mice plotted vs. the effect size of age for all ASPs and those intersecting with genotype (via a main effect and/or interaction), respectively. **f–i** Effect size of genotype in young mice plotted vs. the effect size in old mice for different sets of phenotypes: **g** ASPs ameliorated by genotype via a main effect and/or an interaction. **h** ASPs accentuated by genotype. **i** Phenotypes featuring a genotype main effect and/or a genotype × age interaction but no effect of age. **f** all phenotypes shown in **g–i**. ICC = intraclass correlation. Statistical effect size comparisons were performed via two-sided z-tests. Our analyses are based on unadjusted p -values. Source data are provided as a Source Data file.

allele antagonized this aging-associated phenotype (Fig. 3c). However, we found similar effects of the *Ghrhr*^{fl/fl} allele in old mice as well as in young animals that were younger than the age at which age-dependent changes in this phenotype are first detectable (Fig. 3c). Statistical comparison of genotype effect sizes in young mice vs. effect sizes in old mice revealed only five cases in which there was a significantly larger *Ghrhr*^{fl/fl} effect in the aged group of animals (Fig. 3g), for instance blood hemoglobin concentration or plasma alkaline phosphatase activity. In most cases, however, effect sizes in young and old mice were not significantly different (Fig. 3g; Supplementary Data 7, 8). Hence, based on the analysis of genotype effect sizes in young vs. old mice, only ca. 5.2% of ASPs were countered by the *Ghrhr*^{fl/fl} allele in ways consistent with either the “rate effect model” or “combined rate/baseline effect model” introduced in Fig. 1b (larger effect in old than in young). Ca. 34.4% of all ASPs were countered in ways consistent with

the “baseline effect model” shown in Fig. 1b (effect in old not larger than in young). As mentioned above, the remaining ASPs were either not affected (ca. 36.5%), accentuated (ca. 18.8%) or could not be evaluated (5.2%). Clear correlations between genotype effects within young vs. aged animals were also observed when we analyzed either ASPs accentuated by genotype (Fig. 3h; $ICC = 0.53$, $p = 0.009$), age-insensitive phenotypes influenced by genotype (Fig. 3i; $ICC = 0.73$, $p = 2.10E-07$) or all of these categories combined (Fig. 3f; $ICC = 0.75$, $p = 2.74E-19$). Together, these observations indicate that *Ghrhr* genotype effects were, overall, largely independent of age and this was the case for the set of ASPs countered by genotype and other phenotypic categories (Fig. 3f–i).

Our studies in *Ghrhr*^{fl/fl} mice showed a range of physiological consequences of *Ghrhr* loss of function and highlighted how a subset interacts with age-dependent alterations in mice. We also wanted to



explore whether *GHRHR* expression differences are associated with phenotypic consequences in humans and, if so, whether these effects are age-dependent or not (Fig. 5a–d, Supplementary Table 5). To address this question, we analyzed multi-dimensional phenotypic data, covering a range of areas of human physiology (such as body composition, body fat distribution, cardiology, clinical chemistry,

hematology, inflammation, immunology, muscle strength, ophthalmology and physical activity), collected from $n = 3034$ 30- to 95-year old human individuals (Supplementary Table 6). We identified *GHRHR*-sensitive phenotypes by stratifying the human phenotypic data by *GHRHR* genotype, taking advantage of a SNP (rs11772180), which is located upstream of the *GHRHR* gene and has been identified as an

Fig. 4 | PAAls – standardized coefficients with 95% confidence intervals for age, intervention and intervention × age interaction terms. Phenotypes analyzed within the *Ghrhr*^{lit/lit}, *mTOR*^{KI/KI} and IF cohorts are denoted in blue, green and red, respectively. The forest plots show, for all three PAAls examined in the present paper, standardized coefficients, with 95% confidence intervals, corresponding to the age effects (a, d, g), intervention effects (b, e, h) and intervention × age interactions (c, f, i) derived from linear models applied to all continuously distributed phenotypes included in the present study. Note that we have not included

phenotype labels on the y-axes to allow for a compact data presentation. Phenotypes were sorted based on the coefficient of the age effect. For a given intervention, this order is preserved across all panels from left to right (showing age effects, intervention effects and intervention × age interactions) to permit comparison of coefficients across any given phenotype. Sample sizes (number of mice per group) underlying these analyses are detailed, for each phenotype and all PAAls, in Supplementary Data 8, 10 and 13.

independent cis-eQTL, i.e. a polymorphism significantly associated with *GHRHR* expression levels (Supplementary Fig. 8)⁷⁶. This eQTL had significant effects on several age-sensitive phenotypes examined, including platelet count and cholesterol-associated measures (Fig. 5a–d). In one of these ASPs, the *GHRHR* variant associated with low expression appeared to influence the ASP in ways that counter the direction of age-dependent change (Fig. 5b); there was no genotype × age interaction (Fig. 5b; Supplementary Table 5), which is in line with our observation of predominantly age-independent *Ghrhr* effects on ASPs (including ASPs counteracted by genotype) in mice.

Together, these data indicate that changes in growth hormone signaling are associated with a range of phenotypic effects, including a subset of effects that counteract age-dependent changes. Our data support that most effects on ASPs are evident already in young animals, long before age-dependent changes in ASPs are detectable, indicating that these are age-independent effects. We also identified ASPs that were influenced by the *Ghrhr*^{lit} allele and showed larger effect sizes in old mice than in young mice. These ASPs potentially correspond to phenotypes in which aging trajectories were slowed by the *Ghrhr* mutation.

A hypomorphic *mTOR* mutant allele attenuated ASPs via a mixture of age-independent effects and effects that were more pronounced in old mice

We then asked whether the pattern of observations in the *Ghrhr* mouse model would hold true for other candidate longevity interventions as well. We applied the same analytical approach to a hypomorphic *mTOR* mutant mouse line featuring *mTOR* expression levels reduced to 25% of those seen in WT littermate controls⁵⁷ (Fig. 6; Supplementary Figs. 5, 6; Supplementary Data 9, 10). PCA-based dimensionality reduction of deep phenotyping data from young and old hypomorphic *mTOR* mutant mice as well as WT littermate controls suggested that age and genotype effects in 2D-PCA space are largely independent of each other (Fig. 6b). However, interestingly, the distance between the young and old groups of mice appeared reduced in the case of *mTOR* mutant mice relative to WT controls (Fig. 6b).

Analyses of 208 individual phenotypes covered in these studies identified 117 phenotypes with a significant main effect of age, 98 with a significant main effect of genotype and 45 with a significant interaction between genotype and age (Fig. 6c). Out of the 117 age-sensitive phenotypes, 42 were not significantly affected by genotype, 45 showed a significant main effect of genotype (but no interaction) and 30 featured a significant genotype × age interaction (Fig. 6c). Further analyses of ASPs based on the results of posthoc tests are described in Supplementary Results, Supplementary Fig. 7 and Supplementary Data 10. Figure 4d–f shows standardized coefficients (with their 95% confidence intervals), corresponding to age effects, genotype effects and genotype × age interactions, derived from linear models applied to all continuously distributed phenotypes included in the study. It illustrates that main effects of genotype are abundant and of relatively large effect size which highlights that it is important to consider age-independent effects.

To assess whether genotype effects counteracted or accentuated age effects, we compared for each phenotype the directionality of Cohen's d effect sizes of age with those of Cohen's d effect sizes of genotype (in the old group of mice). Out of 75 ASPs influenced by

genotype, the clear majority (56) was counteracted by the *mTOR*^{KI/KI} genotype (Fig. 6c; Supplementary Data 9, 10; 15 ASPs were accentuated by the *mTOR*^{KI/KI} genotype; 4 ASPs could not be evaluated because Cohen's d effect sizes could not be computed due to 0 values in the denominator). Interestingly, a sizeable fraction (22 of the 56 ASPs) ameliorated by the *mTOR*^{KI/KI} genotype showed a significant interaction between genotype and age (Fig. 6c). It should be noted, however, that the majority of these 56 ASPs showed a main effect of genotype, without evidence for a significant interaction (Fig. 6c). Further inspection of the ASPs with a significant interaction term (considering the directionality of change) indicated that ca. 16.2% of all ASPs identified correspond to ASPs counteracted by *mTOR*^{KI/KI} in ways consistent with the “rate effect model” or “combined rate/baseline effect model” introduced in Fig. 1b. Based on a significant genotype main effect, but a lack of an interaction, ca. 31.6% corresponded to ASPs consistent with the “baseline effect model” shown in Fig. 1b. The remaining ASPs were not affected (ca. 35.9%), accentuated (ca. 12.8%) by *mTOR*^{KI/KI} or could not be evaluated (ca. 3.4%). All the *mTOR*^{KI/KI}-ameliorated ASPs we were able to evaluate had an age at first detectable departure from young adult baseline of 8 months (Fig. 6c), indicating that all corresponding genotype effects on ASPs in our young cohort are independent of age-related changes in these ASPs.

Effect sizes of *mTOR*^{KI/KI} genotype showed a moderate inverse correlation with effect sizes of age (Fig. 6d, e); this was the case, when effect sizes of genotype in either the old (Fig. 6d) or young (Fig. 6e) group were used for correlation analyses.

Next, we addressed whether genotype effects are similar across age groups within the category of ASPs counteracted in *mTOR*^{KI/KI} mutants ($n = 56$ phenotypes). Linear regression analyses of *mTOR*^{KI/KI} genotype effect sizes in young vs. old animals showed clear correlations (Fig. 6g; $R = 0.69$, $p = 3.95E-09$), suggesting that the *mTOR*^{KI/KI} genotype resulted in overall similar phenotypic consequences on ASPs in young and old mice. This was also supported by the slope of the regression line, which did not significantly differ from 1 (slope estimate: 0.91 ± 0.13 ; 95% CI: 0.65, 1.17; $p = 0.491$). Similar results were obtained using intraclass correlation analyses (Fig. 6g; ICC = 0.67, $p = 5.00E-09$). Statistical comparison of genotype effect sizes in young vs. old mice revealed 11 cases in which there was a significantly larger *mTOR*^{KI/KI} effect in the aged group of animals (Fig. 6g), for instance hematocrit or plasma concentration of triglycerides. In most cases, however, effect sizes in young and old mice were not significantly different (Fig. 6g; Supplementary Data 9, 10). Together, based on the analysis of genotype effect sizes in young vs. old mice, only ca. 9.4% of ASPs were counteracted by the *mTOR*^{KI} allele in ways consistent with either the “rate effect model” or “combined rate/baseline effect model” introduced in Fig. 1b (larger effect in old than in young). Ca. 38.5% of all ASPs were counteracted in ways consistent with the “baseline effect model” shown in Fig. 1b (effect in old not larger than in young). As mentioned above, the remaining ASPs were either not affected (ca. 35.9%), accentuated (ca. 12.8%) or could not be evaluated (3.4%).

We also observed correlations between genotype effects within young vs. aged mice when either analyzing ASPs exacerbated in *mTOR*^{KI/KI} mice (Fig. 6h; ICC = 0.75, $p = 0.0003$) or genotype- but not age-sensitive phenotypes (Fig. 6i; ICC = 0.71, $p = 2.74E-07$), indicating that the *mTOR*^{KI/KI} genotype had overall very similar effects in young

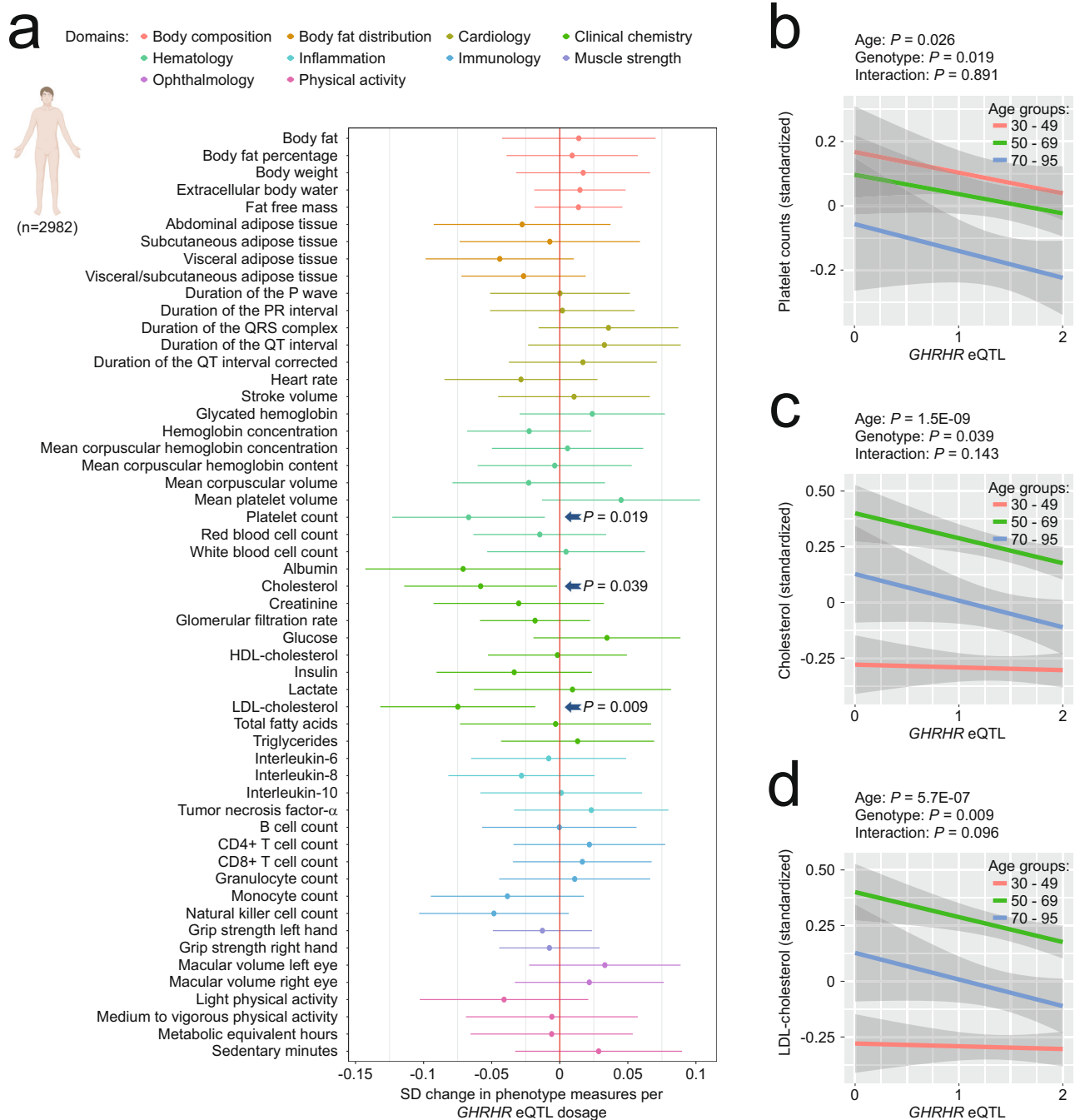


Fig. 5 | GHRHR eQTL effects on aging-associated phenotypes in humans.

a–d Phenotyping results in a large deep-phenotyped human cohort that included participants of both genders with an age range from 30–95 years. **a** Change in phenotype (in standard deviations (SD) from the mean) associated with *GHRHR* eQTL dosage with the horizontal whiskers indicating the 95% confidence intervals of the mean effect estimate; * denotes $p < 0.05$ for the linear association between *GHRHR* eQTL dosage and phenotype. The association between eQTL dosage and each phenotypic measure was assessed using multiple linear regression models adjusted for age, sex and population stratification using the first ten genetic

principal components. Our analyses are based on unadjusted p -values. Change of platelet count (**b**), total cholesterol (**c**) and LDL-cholesterol (**d**) associated with *GHRHR* eQTL dosage in 30–49 years old (red line), 50–69 years old (green line) and 70–95 years old humans (blue line); the lines represent the best-fit least squares regression lines with surrounding 95% confidence intervals of the mean indicated in gray. The eQTL dosage was coded as GG = 0, AG = 1, and AA = 2 (GG is associated with lowest expression levels, AA with highest; see Supplementary Fig. 8a). Sample size was 994 human participants per age group. Created with BioRender.com.

and old mice, irrespective of whether phenotypes were age-sensitive or not.

We next wanted to establish whether transcriptomic effects on age-sensitive genes are similar in young and old *mTOR^{KI/KI}* mice. We performed RNA-seq analyses in spleen tissue of young (~3 months old; i.e., well before the onset of age-dependent transcriptomic changes; see Fig. 2i) as well as old (~20 months old) *mTOR* mutants and WT

littermate controls. These analyses identified 54 genes that were age-sensitive ($FDR < 0.05$) and 855 genes that were genotype-sensitive with an intersection between these populations of 9 genes (Supplementary Fig. 9a; Supplementary Data 11). The overlap of age- and *mTOR*-sensitive genes is greater than expected by chance (representation factor = 4.9, $p = 7.68E-05$). No genes with a significant ($FDR < 0.05$) genotype \times age interaction were detected (Supplementary Fig. 9a). To

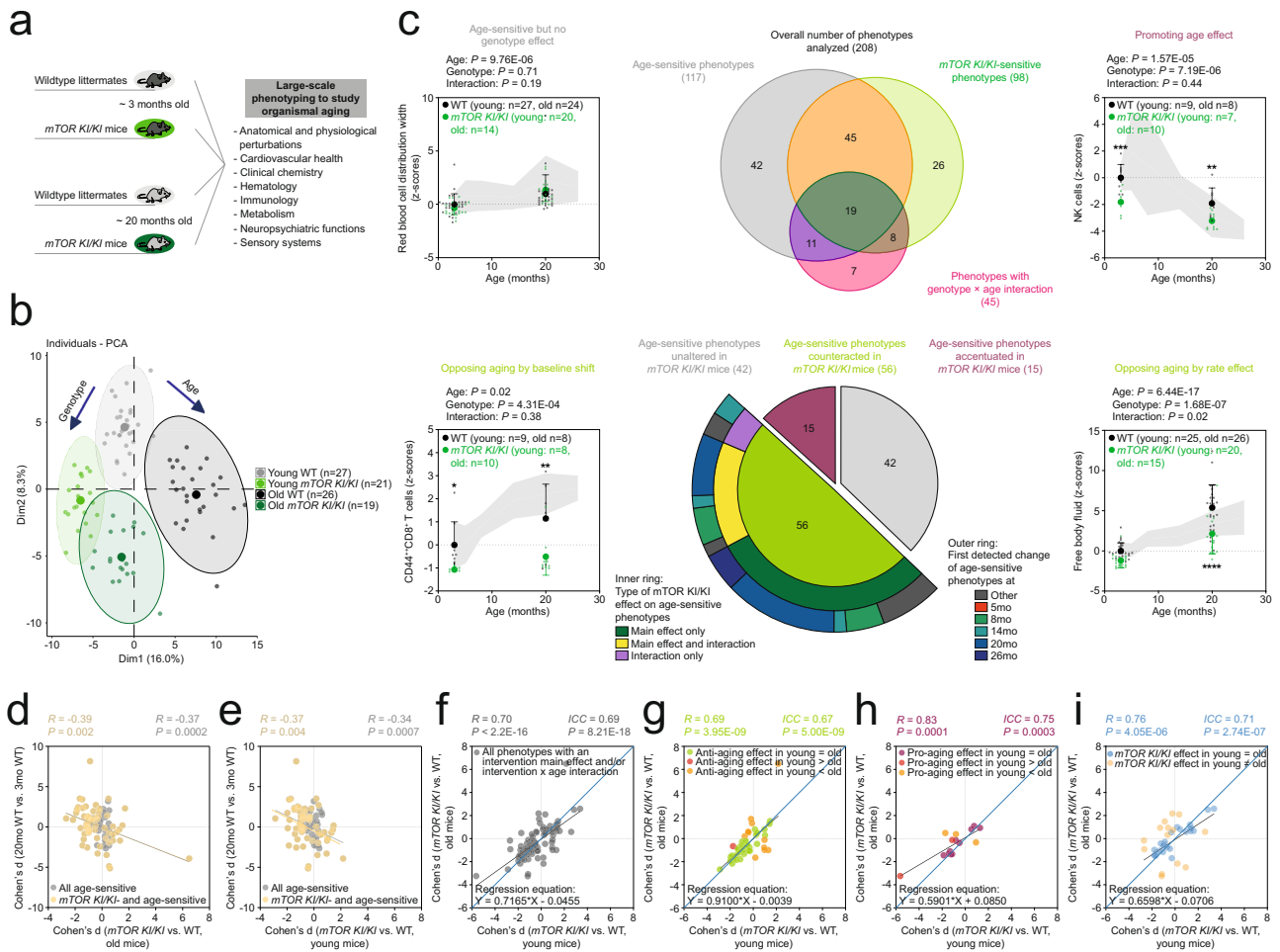


Fig. 6 | A hypomorphic *mTOR* mutant allele attenuated ASPs via a mixture of age-independent effects and effects more pronounced in old mice. a–i Deep phenotyping results in *mTOR^{K1/K1}* mice. **a** Schematic illustration of study design. Mouse symbols adapted from ref. 10. **b** Principal component analysis of deep phenotyping data. **c** Venn diagram shows the number of ASPs, genotype-sensitive phenotypes, phenotypes with a genotype × age interaction and their intersection. Sunburst chart shows the number of ASPs either unaltered, counteracted or accentuated by genotype. For ASPs counteracted by genotype, the inner ring shows the proportion of phenotypes with either a genotype main effect, a genotype × age interaction or both. The outer ring shows when changes in the corresponding ASPs were first detected in our baseline study. Line charts show representative examples of phenotypes influenced by age and/or intervention in the different possible ways. Data are presented as z-scores (normalized to the young WT group) and are plotted as mean ± S.D. (individual data points are superimposed). Two-way ANOVAs with the between-subjects factors age and genotype followed by Fisher’s LSD posthoc

analyses, where appropriate, were used for data analysis. **p* < 0.05, ***p* < 0.01, ****p* < 0.001 relative to age-matched wildtype littermate controls. Life-time trajectories of the corresponding phenotypes, representing measurements obtained in our baseline study, are shown by the gray-shaded area in the background (bounded by mean ± S.D.). Effect size of genotype in old (d) or young (e) mice plotted vs. the effect size of age for all ASPs and those intersecting with genotype (via a main effect and/or interaction), respectively. f–i Effect size of genotype in young mice plotted vs. the effect size in old mice for different sets of phenotypes: g ASPs ameliorated by genotype via a main effect and/or an interaction. h ASPs accentuated by genotype. i Phenotypes featuring a genotype main effect and/or a genotype × age interaction but no effect of age. f All phenotypes shown in g–i. ICC = intraclass correlation. Statistical effect size comparisons were performed via two-sided z-tests. Our analyses are based on unadjusted *p*-values. Source data are provided as a Source Data file.

assess whether the *mTOR* mutant allele counteracted or accentuated age-dependent gene expression alterations in spleen, expression levels were compared between young and old *mTOR* mutants and WT littermate controls. Aging-associated changes of five genes were counteracted and age-related alterations of four genes were accentuated in the *mTOR^{K1/K1}* mice (Supplementary Fig. 9b).

We also wanted to explore how altered *MTOR* expression may affect age-sensitive phenotypes in human subjects. We assessed the associations between multi-dimensional phenotypic human data with polymorphisms at a SNP in the promoter region of the *MTOR* gene (rs2295079) that has previously been associated with variations in *MTOR* expression levels (Supplementary Fig. 8)⁷⁶. Out of 54 phenotypes (Fig. 7a), we identified 5 (Fig. 7a–f) to be associated with variations in *MTOR* eQTL, including body fat content (Fig. 7b, c) and body weight (Fig. 7d), which are known to be sensitive to changes in *mTOR*

function^{16,57,77}. Next, for these 5 *MTOR*-sensitive phenotypes, we examined whether the effects of *MTOR* eQTL was age-specific or not. For 3 out of 5 parameters, we found significant effects of *MTOR* eQTL as well as of age, but no genotype × age interaction (Fig. 7d–f; Supplementary Table 7), suggesting that *MTOR* eQTL was largely associated with similar effects in younger and older individuals. Two phenotypes (body fat and % body fat) showed a significant genotype × age interaction which appeared to be driven by an *MTOR* variant effect in the youngest group of individuals (Fig. 7b, c; Supplementary Table 7). The *MTOR* variant associated with low expression appeared to influence some age-sensitive phenotypes in ways that counter the direction of age-dependent change (Fig. 7b, c, e). In other cases, age and genotype effects were in the same direction (Fig. 7d, f). Altogether our *mTOR*-based analyses in mouse and humans indicate that *mTOR* effects on age-sensitive phenotypes (including ASPs counteracted by

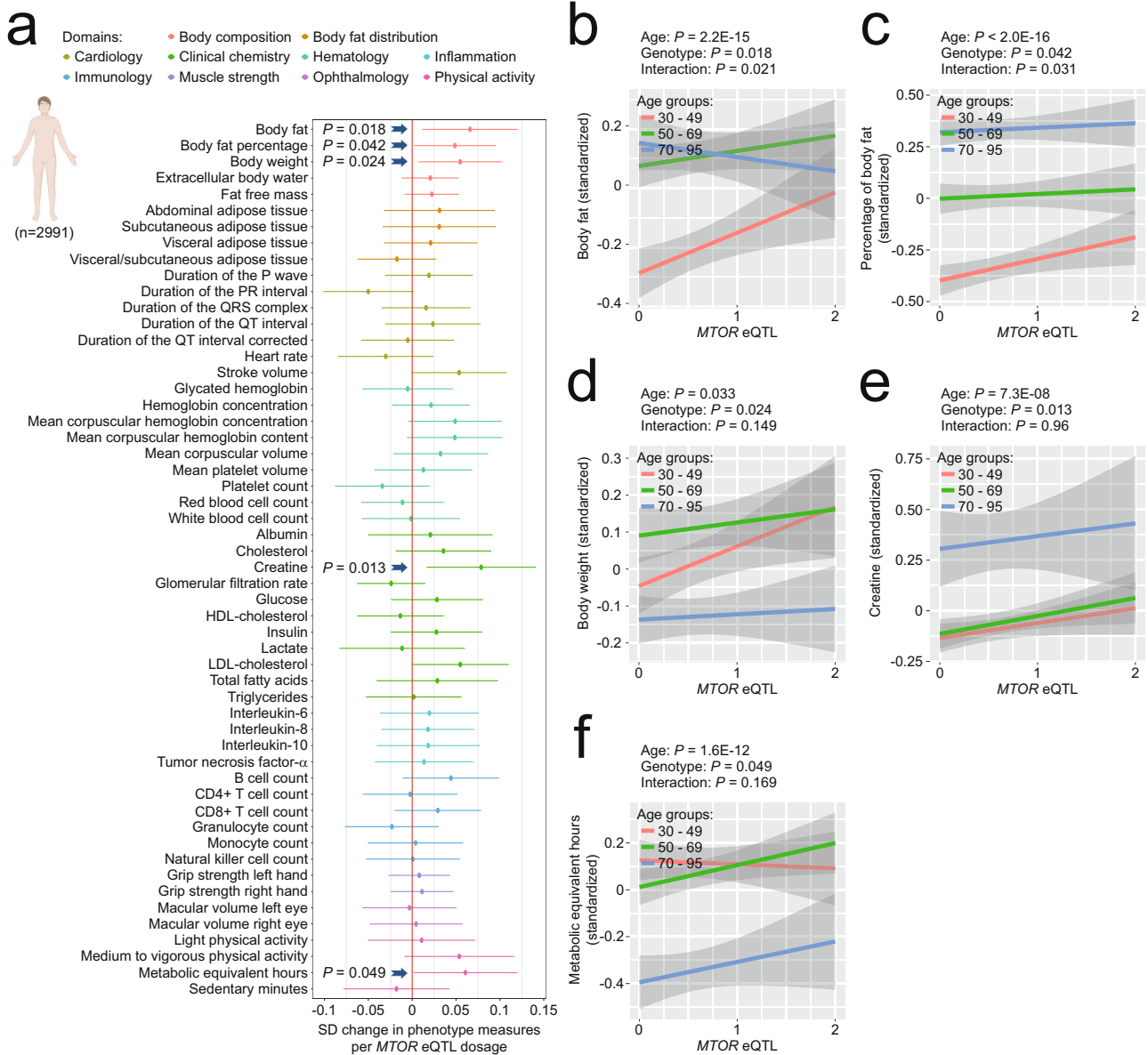


Fig. 7 | *MTOR* eQTL effects on aging-associated phenotypes in humans. **a–f** Phenotyping results in a human cohort that included participants of both genders with an age range from 30–95 years. **a** Change in phenotype associated with *MTOR* eQTL dosage in a large deep-phenotyped human cohort, with the horizontal whiskers indicating the 95% confidence intervals of the mean effect estimate; * denotes $p < 0.05$ for the linear association between *MTOR* eQTL dosage and phenotype. The association between eQTL dosage and each phenotypic measure was assessed using multiple linear regression models adjusted for age, sex and population stratification using the first ten genetic principal components. Our

analyses are based on unadjusted p -values. Change of body fat (**b**), percentage of body fat (**c**), body weight (**d**), plasma creatine concentration (**e**) and metabolic equivalent hours (**f**) associated with *MTOR* eQTL dosage in 30–49 years old (red line), 50–69 years old (green line) and 70–95 years old humans (blue line); the lines represent the best-fit least squares regression lines with surrounding 95% confidence intervals of the mean indicated in gray. The eQTL dosage was coded as GG = 0, CG = 1, and CC = 2 (GG is associated with lowest expression levels, CC with highest; see Supplementary Fig. 8b). Sample size was 997 human participants per age group. Created with BioRender.com.

mTOR effects) are often similar in young and old groups; accordingly, age-independent mechanisms need to be taken into account when interpreting mTOR effects on age-sensitive parameters.

An intermittent fasting-based variant of dietary restriction ameliorated ASPs frequently through age-independent mechanisms

While genotype \times age interactions were also observed, the data summarized above endorses an important role of age-independent effects on ASPs in the context of two central genetic interventions, targeting *mTOR* or *Ghrhr*. We also applied our analytical approach to a major environmental factor studied in aging and longevity - dietary

restriction^{78,79}. Specifically, we assessed whether and to what extent age-dependent phenotypic changes in mice are ameliorated by intermittent fasting (IF)/every other day feeding (EOD) (for details regarding study design, see Fig. 8a and Methods section). We had previously reported a significant lifespan extension induced by IF in this cohort of mice¹⁰. Food intake, body weight and body composition data have also been previously reported¹⁰. PCA of all deep phenotyping data revealed an additive nature of age and IF effects (Fig. 8b); PC1 was shifted to the right by age in both groups. Fasting acted mainly by decrem-

ing PC2. Analyses of individual phenotypes (157) revealed 102 with a significant main effect of age, 74 with a significant main effect of diet and

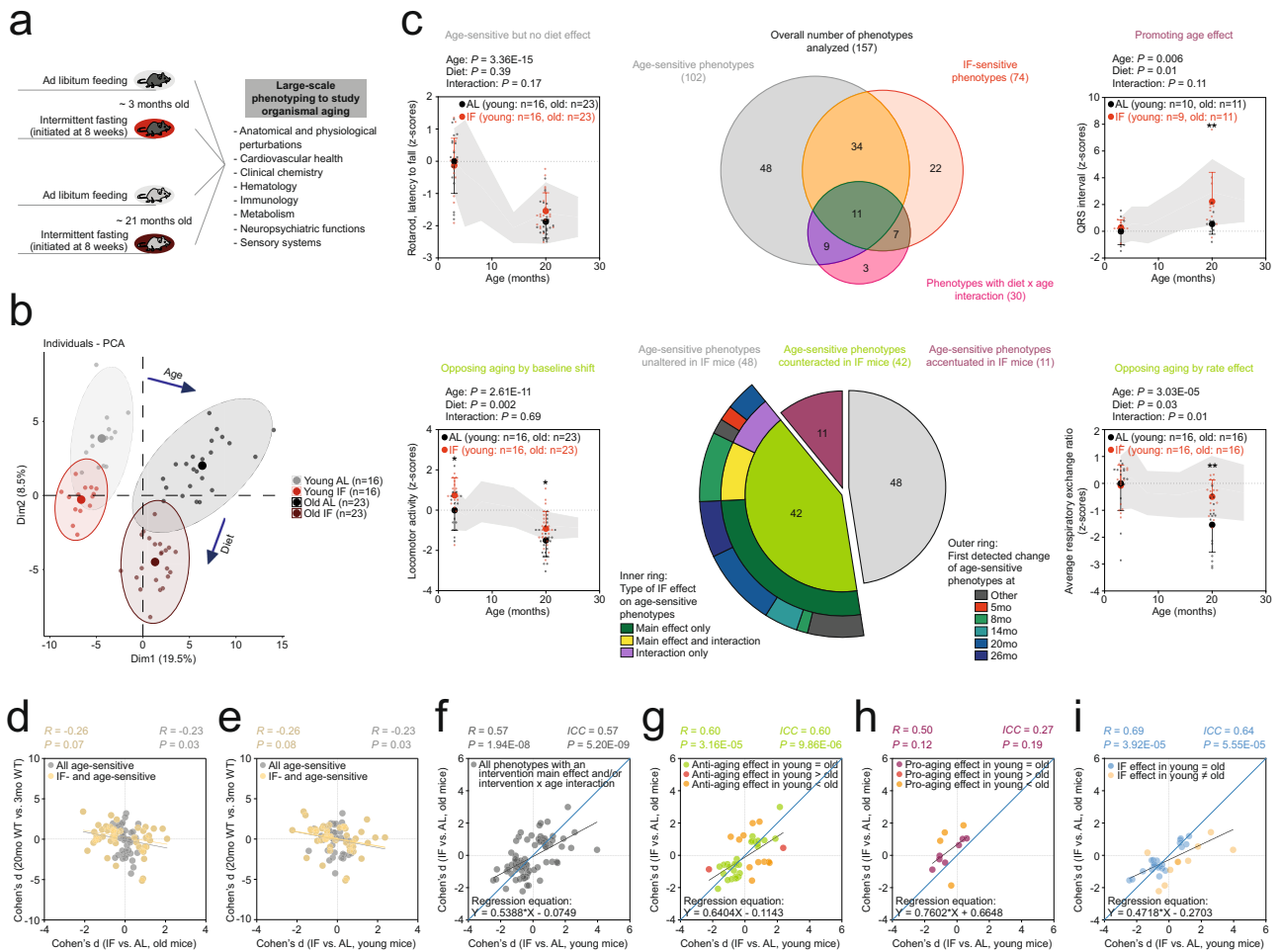


Fig. 8 | ‘Anti-aging’ effects induced by intermittent fasting (IF) often manifest in young mice (prior to detectable age-dependent phenotypic changes). **a–i** Deep phenotyping results in IF mice. **a** Schematic illustration of study design. Mouse symbols adapted from ref. 10. **b** Principal component analysis of deep phenotyping data. **c** Venn diagram shows the number of ASPs, diet-sensitive phenotypes, phenotypes with a diet × age interaction and their intersection. Sunburst chart shows the number of ASPs either unaltered, counteracted or accentuated by diet. For ASPs counteracted by diet, the inner ring shows the proportion of phenotypes with either a diet main effect, a diet × age interaction or both. The outer ring shows when changes in the corresponding ASPs were first detected in our baseline study. Line charts show representative examples of phenotypes influenced by age and/or intervention in the different possible ways. Data are presented as z-scores (normalized to the young WT group) and are plotted as mean ± S.D. (individual data points are superimposed). Two-way ANOVAs with the between-subjects factors age

and diet followed by Fisher’s LSD posthoc analyses, where appropriate, were used for data analysis. **p* < 0.05, ***p* < 0.01, ****p* < 0.001 relative to age-matched wildtype littermate controls. Life-time trajectories of the corresponding phenotypes, representing measurements obtained in our baseline study, are shown by the gray-shaded area in the background (bounded by mean ± S.D.). Effect size of diet in old (**d**) or young (**e**) mice plotted vs. the effect size of age for all ASPs and those intersecting with diet (via a main effect and/or interaction), respectively. **f–i** Effect size of diet in young mice plotted vs. the effect size in old mice for different sets of phenotypes: **g** ASPs ameliorated by diet via a main effect and/or an interaction. **h** ASPs accentuated by diet. **i**, Phenotypes featuring a diet main effect and/or a diet × age interaction but no effect of age. **f** all phenotypes shown in **g–i**. ICC = intraclass correlation. Statistical effect size comparisons were performed via two-sided z-tests. Our analyses are based on unadjusted *p*-values. Source data are provided as a Source Data file.

30 with a significant diet × age interaction (Fig. 8c; Supplementary Fig. 5; Supplementary Data 12, 13). Out of the 102 phenotypes with a main effect of age (ASPs), 48 were not significantly influenced by diet, 34 showed a significant main effect of diet (but no interaction) and 20 featured a significant diet × age interaction. Further analyses of ASPs based on the results of posthoc tests are described in Supplementary Results, Supplementary Fig. 7 and Supplementary Data 13. Figure 4g–i presents standardized coefficients (with their 95% confidence intervals), corresponding to age effects, diet effects and diet × age interactions, derived from linear models applied to all continuously distributed phenotypes included in the study. The figure shows that main effects of diet are common and of relatively large effect size, highlighting the overall important role of age-independent effects on ASPs and other phenotypes.

Next, we wanted to more closely examine ASPs influenced by diet (either via a main effect or a diet × age interaction). To do so, we

computed Cohen’s d effect sizes of age and of diet (in the old cohort of mice) to examine whether they acted in opposing directions or not (Fig. 8c). These analyses showed that age and diet effects operated in opposing directions in 42 cases; 11 ASPs were exacerbated by IF; 1 ASP could not be evaluated because Cohen’s d effect sizes could not be computed due to a 0 value in the denominator. Most of the 42 ASPs countered by IF showed a significant main effect of diet, but no significant interaction between diet and age (Fig. 8c). Further analysis of the ASPs featuring a significant interaction term (considering the directionality of change) indicated that ca. 13.7% of all ASPs identified correspond to ASPs counteracted by IF in ways consistent with the “rate effect model” or “combined rate/baseline effect model” introduced in Fig. 1b. Based on a significant genotype main effect, but a lack of an interaction, ca. 27.5% corresponded to ASPs consistent with the “baseline effect model” shown in Fig. 1b. The remaining ASPs were not affected (ca. 47.1%), accentuated (ca. 10.8%) by IF or could not be

evaluated (ca. 1%). Most of the IF-attenuated ASPs examined had an age at first detectable departure from the young adult baseline of 8 months (Fig. 8c), implying that corresponding IF effects on ASPs in our young group are independent of age-related change in those ASPs.

Correlation analyses of diet effect sizes in old (Fig. 8d) and young (Fig. 8e) mice vs. effect sizes of age showed a modest inverse correlation, which is consistent with an antagonistic relationship between IF and aging.

We examined whether diet effects are similar across age groups within the category of ASPs counteracted by IF ($n = 42$ phenotypes). Correlation analyses of IF effect sizes in young vs. old mice showed a significant positive relationship for ASPs antagonized by diet (Fig. 8g; $R = 0.60$, $p = 3.16 \times 10^{-5}$), indicating that ASPs in young and old animals were affected by IF in similar ways. The slope of the regression line was 0.64 ± 0.14 (95% CI: 0.36, 0.92; $p = 0.0119$), indicating that effects overall did not tend to be larger in old mice than in young mice. Similar results were obtained using intraclass correlation analyses (Fig. 8g; ICC = 0.60, $p = 9.86 \times 10^{-6}$) which reflect not only the degree of correlation but also the agreement between measures in the young and old group. Statistical comparison of genotype effect sizes in young mice vs. effect sizes in old mice showed that in 31 out of 42 cases effect sizes in young and old mice were not significantly different (Fig. 8g; Supplementary Data 12, 13). For instance, in agreement with previously published data^{16,70,80,81}, advanced age was associated with decreased exploratory locomotor activity in a novel environment and this aging-associated phenotype was antagonized by IF (Fig. 8c). We identified 11 phenotypes with significantly larger effect sizes in old mice than in young mice (Fig. 8g; Supplementary Data 12, 13), for example average respiratory exchange rate or NKT cell count. Based on the analysis of genotype effect sizes in young vs. old mice, ca. 10.8% of ASPs were counteracted by IF in ways consistent with either the “rate effect model” or “combined rate/baseline effect model” introduced in Fig. 1b (i.e., larger effect in old than in young). Ca. 30.4% of all ASPs were counteracted in ways consistent with the “baseline effect model” shown in Fig. 1b (i.e., effect in old not larger than in young). As mentioned above, the remaining ASPs were either not affected (ca. 47.1%), accentuated (ca. 10.8%) or could not be evaluated (1%).

Finally, we wanted to address to what extent the phenotypes used in our analyses are potentially interrelated. To address this, we performed hierarchical clustering on the phenotypic data from the young control groups for each of our three intervention studies (Supplementary Figs. 10–12; Supplementary Data 14–16). These analyses revealed the expected consistently low distances between phenotypes known to be related, such as e.g. peripheral blood hemoglobin concentration and hematocrit. However, they also show relatively large distances between many of the phenotypes, suggesting that much of the variation in the data would be lost if our analyses were restricted to a small subset of phenotypes only. Analyses of intervention influences on clusters (based on different cluster definitions) are summarized in Supplementary Data 14–16.

For all PAAIs assessed in the present study, pro-longevity effects have been demonstrated previously^{10,35,60}. We have shown IF-induced lifespan extension in a prior study¹⁰ that was carried out side-by-side with the collection of the aging data on which the current analyses are based. Although our present experiments were not designed to ascertain pro-longevity effects (which would have required aging substantially larger groups of animals over longer time periods), provisional survival estimates based on animals aged in our facility are not inconsistent with previously reported pro-longevity effects of the *Ghrhr^{lit/lit}* and *mTOR^{KI/KI}* genotype, respectively (Supplementary Fig. 6). Moreover, comprehensive macropathological and histopathological analyses revealed significantly reduced tumor burden in *mTOR^{KI/KI}* and *Ghrhr^{lit/lit}* mutants relative to their wildtype littermate controls (Supplementary Fig. 6), which is consistent with earlier findings in *mTOR^{KI/KI}*/*K^{BS}* and dwarf mice^{47,82}, respectively. Neoplastic disease is a major

factor in limiting natural lifespan in C57BL/6J animals as well as other stocks of mice^{5–10}.

As outlined above, aging and neoplastic disease often are overlapping conditions. We deliberately made no attempt to pre-select animals (for inclusion in our study) based on their apparent fitness or health status as this could have complicated the interpretation of our findings. For instance, if a longevity intervention does not improve age-sensitive phenotypes in a pre-selected set of healthy mice, this observation is difficult to interpret: Possibly, the intervention has truly no effects on age-sensitive phenotypes but, alternatively, differential inclusion could confound this analysis (e.g. controls with the poorest aging outcomes may have been excluded from the analysis and, hence, cannot be analyzed, while mice with poor - but not sufficiently poor to lead to exclusion - aging outcomes may still be existing in the intervention group, thereby resulting in a biased estimate of aging outcomes across these two populations). Nonetheless, in order to address whether neoplastic disease could have influenced some of our parameter estimates in aging mice, we subjected all animals to a macropathological assessment after completion of phenotypic analyses. Repeating the analyses outlined above on the tumor-free (i.e., free of macropathologically detectable tumors) set of mice revealed qualitatively similar results compared to the entire set of animals (Supplementary Figs. 13–16; Supplementary Data 2, 8, 10, 13), suggesting that key observations of our study also hold up when considering only aged animals that are free of detectable neoplastic disease.

Altogether, our deep phenotyping analyses based on three different central longevity interventions revealed that intervention-sensitive ASPs are in many cases influenced in age-independent ways, with similar effects in aged mice and in animals younger than the age of onset of change in the corresponding phenotypes. These observations provide support for the view that age-dependent phenotypic change in these cases is not broadly slowed by these interventions. Rather, ASPs tend to alter the point of departure under these interventions; the progression of aging remains unaltered in these cases. We also identified some phenotypes that were predominantly influenced by PAAIs in old mice (with more limited or no clear effects in young mice). These cases represent phenotypes in which the progression of age-related change appears to be modified by PAAIs, consistent with a slowed rate of aging.

Discussion

Lifespan studies provide insights about factors that naturally limit lifespan. In many strains of mice (including C57BL/6J), cancers represent the main life-limiting factor accounting for 70–90% of all natural causes of death^{5–10}. Hence, studying PAAIs in the context of lifespan analyses in mice will primarily promote our understanding of how PAAIs interact with cancers but will not address whether PAAIs influence age-sensitive phenotypes (ASPs) that do not limit lifespan (i.e., most ASPs). Based on these considerations, it is a misconception that lifespan data alone can be used as a powerful proxy for the study of organismal aging in mice⁸³. Rather, age-dependent phenotypic change, including all its many facets, has to be studied directly.

We herein defined aging trajectories of hundreds of phenotypes and thousands of molecular markers across the lifespan of male C57BL/6J mice. Our newly established atlas revealed that most ASPs showed relative stability in young adulthood (between 3 and 5 months of age). Moreover, age-dependent changes in ASPs mostly began to be detectable in the second year of life in our dataset. These data serve as a critical resource for the proper interpretation of the nature of anti-aging effects induced by genetic, pharmacological or dietary interventions in mice.

We also analyzed central genetic and environmental longevity regulators (putative anti-aging interventions; PAAIs) for their mechanistic influences on hundreds of phenotypes in young and old cohorts of animals. Integration of these data with our aging trajectory

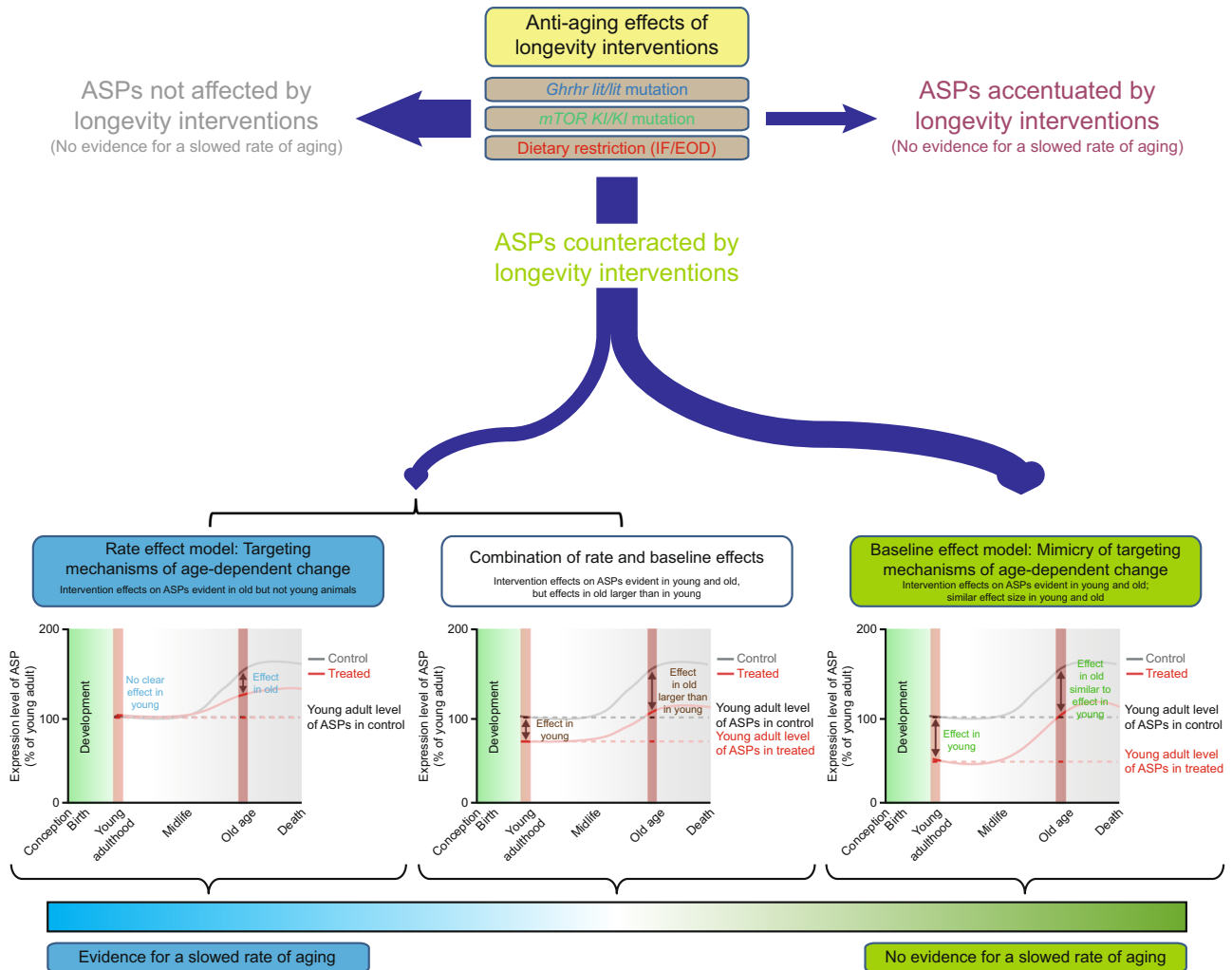


Fig. 9 | ‘Anti-aging’ effects were frequently age-independent in nature. The schematic illustrates major scenarios by which PAAls could influence aging phenotypes. First, interventions could have no measurable effect on a set of phenotypes or even accentuate age-dependent phenotypic change. ASPs countered by an intervention could be influenced in ways consistent with a targeting of the mechanisms underlying age-dependent phenotypic change: In this case, PAAI effects should become apparent only after the onset of aging-associated phenotypic change, but not at younger ages (rate effect). PAAI effects at a young age

(prior to the age when age-dependent phenotypic change becomes first detectable) indicate that it is not the age-dependent change that is being targeted (baseline effect). Although our studies revealed examples of both rate and baseline effects, many ‘anti-aging’ effects fell into the latter category (age-independent effects that do not provide evidence for a slowed aging rate). Ignoring this distinction would lead to a substantial overestimation of the extent by which PAAls slow the aging process. Created with BioRender.com.

dataset revealed that many intervention effects were clearly measurable not only in the old but also, with similar effect sizes, in the young cohorts of mice, at an age long before age-dependent changes in ASPs began to be detectable. Accordingly, these PAAI effects cannot be taken as evidence that the PAAls slowed aging (age-dependent change). These observations are consistent with data we obtained in humans that also showed age-independent effects on age-sensitive phenotypes of *GHRHR* and *MTOR* genetic variants. In addition to ASPs that were influenced in age-independent ways, we also identified smaller subsets of ASPs that were predominantly affected in the old cohort of animals, suggesting that PAAls may potentially target age-dependent changes in these traits. Hence, our dataset allowed us to isolate different modes of actions (age-independent vs. age-dependent influences) of PAAls acting on different ASPs.

Prevailing molecular damage theories of aging posit that aging is fundamentally caused by the age-dependent accumulation of molecular damage linked to progressive telomere shortening, accumulation of misfolded proteins, genomic instability, epigenetic changes, increased numbers of senescent cells, metabolic dysfunction, progressive and irreversible changes of the extracellular matrix, etc.⁴.

However, one current limitation of these concepts of the biology of aging is that they are largely based on lifespan data or on analyses of aging traits more limited in scope than the present study. There is also in particular a shortage of studies in mammalian models and of research that considers the controls we built in the present work to account for possible age-independent PAAI effects. Contrary to a general expectation that ‘anti-aging’ treatments should produce a broad change in aging rate across many phenotypes^{33,36,53,70,72,84–91}, our study shows that the PAAls we examined - that are concerned with some of the very core mechanisms proposed to be involved in aging⁴ - did often not seem to work through targeting age-dependent change (Fig. 9). This is not to say that we did not observe individual anti-aging effects that were consistent with a slowed aging rate; parameters that followed this pattern did, however, represent the minority of cases of anti-aging influences observed in the present study. We were able to come to this conclusion because, unlike many prior studies, we had included young treated (mutant, fasted) groups in our study design and determined the age at which phenotypic change began to be detectable for the parameters examined. Had we not done this, we would have substantially overestimated PAAI effects on the

progression of aging. We recommend that comprehensive phenotyping, including the controls built in our study, should be adopted in future work investigating PAAIs, since this facilitates the proper interpretation of the mechanistic mode by which PAAIs influence biological aging. Our observations then suggests that we should not be looking for generalized rate effects of PAAIs (which one would expect if there was a centralized process regulating aging rate that was being targeted by a PAAI), but rather expect more specific effects on subsets of aging phenotypes (which one would expect if a PAAI targets more decentral processes). It is also important to acknowledge that all PAAIs examined in the present study exerted pro-aging effects on a subset of ASPs. Note that pro-aging effects were roughly balanced with anti-aging effects (Ghrhr: 10.4% of ASPs with anti-aging influences vs. 18.8% with pro-aging effects; mTOR: 16.2% anti-aging vs. 12.8% pro-aging; IF: 27.5% anti-aging vs. 10.8% pro-aging; for further details, see Results section above). Together, our observations are not in line with the view that these PAAIs have broad, or even generalized, ‘anti-aging’ effects.

The inclusion of young intervention controls is critical to avoid potential misinterpretations in studies assessing PAAI effects on aging. Consider the following analogy: A treatment (e.g., an oral treatment with caffeine) improves memory performance in subjects affected by Alzheimer’s disease (AD). The same treatment however also leads to a rapid improvement in memory performance in healthy young adults (with the same effect size as in the AD subjects). The most parsimonious explanation for this pattern of findings is that they reflect a symptomatic treatment effect (because the effect is also seen in individuals who don’t have the disease). This finding cannot be used to claim that caffeine slows the pathogenesis of AD.

Here, we generated data on PAAI effect sizes in young and old animals for all of the many phenotypes we examined and then applied the logic outlined in the example above to our entire dataset. While we were able to detect some ASPs that showed larger PAAI effect sizes in old animals than in young animals, we noted that there were many ASPs that were already affected in young animals (with similar effect sizes as in old animals), long before any age-dependent change in these ASPs becomes apparent. Unlike our study, many prior analyses did not include young PAAI groups. They erroneously concluded that interventions slowed aging based only on the observation that old treated animals look on some ASPs more like young controls than the old control animals do. This would be like concluding that caffeine slows the progression of AD in our example above.

The distinction between symptomatic and causal effects on aging is of fundamental importance, yet is often ignored. Claiming that an intervention “slows aging” simply based on a reduction of specific age-related pathologies or other age-related features is not sufficient. Supplementary Fig. 17 and the remainder of this paragraph explain the importance of this distinction using the age-related pathology “cancer” as an example, but please note that similar arguments could be made for any other age-related pathology (or any other age-related feature): The increased risk for aged individuals to develop cancers is due to specific factors, such as a loss of genomic stability/the mutational burden that accumulates during tissue aging. A PAAI that truly slows aging (i.e., that slows aging in a causal sense) has to tackle the root causes underlying age-dependent change in phenotype. Accordingly, the PAAI (hereafter called PAAI_causal) would have to prevent genomic instability/mutation accumulation which underlie the aging-associated cancer predisposition in our example (Supplementary Fig. 17). Importantly, a PAAI could also inhibit cancers in symptomatic ways, i.e., by tapping into mechanisms unrelated to the ones that mechanistically link aging and cancer formation (hereafter called PAAI_symptomatic). For instance, cytostatic drugs may be used to inhibit cancers via a general inhibition of cell proliferation, while leaving genomic instability/mutation accumulation unaffected (or even

enhancing genomic instability due to mutagenic properties that can be associated with this class of drugs) (Supplementary Fig. 17). Note that both of the PAAI scenarios discussed above could cause aged animals to have a lower cancer burden (Supplementary Fig. 17). However, it would not be meaningful to consider the animals treated with PAAI_symptomatic to benefit from “slowed aging” given that they are as cancer-prone as untreated age-matched controls (or perhaps even more cancer-prone due to potential mutagenic effects of cytostatic drugs) and this would become apparent as soon as the symptomatic treatment is stopped. Animals subjected to PAAI_causal, in contrast, would show a causal reduction in cancer risk (explained by preserved genomic integrity) which persists even beyond termination of treatment.

The molecular and cellular mechanisms underlying aging-associated phenotypic changes, examined in the present study, are currently still poorly defined; they are likely complex and may vary from phenotype to phenotype^{15,92}. Importantly, our approach does not require knowledge of the mechanisms underlying age-dependent change. In the absence of this knowledge, using the approach outlined in this paper, we are still able to address whether PAAIs may act by targeting age-dependent phenotypic change. It will be an important challenge for future research to define the underlying mechanisms. Our findings also suggest that a reexamination of the ‘hallmarks of aging’ processes⁴, using large-scale phenotyping with the controls outlined in this paper, is warranted to address whether these processes indeed broadly regulate aging or are primarily the ‘hallmarks of lifespan’ with more limited roles in aging.

Our observations are consistent with early considerations by Richardson & Carter who noted that, among a handful of age-sensitive phenotypes responsive to caloric restriction (CR), CR effects were seen in young animals as well, indicating that in these cases CR shifted the level of the process and did not affect the rate of age-dependent change¹⁹. Our deep phenotyping approach places this notion on a solid foundation (we analyzed hundreds of phenotypes) and extends this early consideration to IF-based models of dietary restriction as well as central genetic models of longevity, targeting mTOR and growth hormone signaling pathways. Our findings, therefore, raise the possibility that the age-independent nature of ‘anti-aging’ effects may be common among longevity interventions. This would imply that many ‘anti-aging’ effects are unlikely to arise from targeting the causal factors driving aging.

Our findings are in agreement with the notion that genetic effects tend not to be strictly age-specific but mostly affect the organism across its lifespan⁹². Accordingly, given that our PAAIs often had effects in young individuals, which were frequently of similar effect size as those in old subjects, relatively shorter-term exposure to treatment may to some extent be sufficient to induce sizeable PAAI effects at a young age. Therefore, an important next step is to address whether PAAIs can also induce sizeable treatment effects when old individuals with established phenotypic change are subjected to short-term interventions. This may substantially simplify the development of therapeutics because of shortened treatment periods and the possibility that treatment may, at least in some cases, come with therapeutic benefit even after the onset of age-dependent change. These treatments would be considered symptomatic, not causal, in nature but may still provide valuable alleviation of a subset of aging phenotypes.

Our study has some limitations. We did not use a longitudinal study design to infer aging trajectories and intervention effects. Rather, we employed a cross-sectional study design that compared different sets of mice to extract age and intervention effects. While longitudinal analyses have their strengths (i.e., being able to take repeated measurements on the same animal, at least for the sets of phenotypes where repeated measurements are possible), they are

certainly not without complications and have their own sets of limitations: An important complication of performing assays within longitudinal designs are order effects, referring to the phenomenon that having been tested once or more times has effects on the outcome of subsequent tests (e.g., in behavioral assays). Another important issue inextricably linked to longitudinal designs is that measurements cannot be taken at the same time but instead require comparison of data collected at different points in time (which would be up to 2 years apart in our study). Hence, although there may be exceptions depending on what parameters one specifically considers, longitudinal data may not necessarily generate more robust estimates of aging trajectories in mouse populations than population estimates derived from cross-sectional data collected at the same time, by the same person and under the same well-controlled conditions. Please also note that a considerable number of parameters we measured was collected in the context of terminal procedures, precluding repeated data collection from the same animal. In line with all of these considerations, it is common practice to infer aging trajectories from studies using cross-sectional designs^{93–98}.

One goal of our analyses was to estimate, using pairwise comparisons against the 3-month old group, when mouse phenotypes show first measurable departures from our young adult baseline (i.e., from the 3-month old group). Note that the sensitivity to detect differences between these groups (i.e., the limit of detection) depends on sample size. Increasing sample size could almost arbitrarily lower the limit of detection and potentially reveal additional smaller-sized group differences if they exist.

We identified a number of ASPs that appeared to be affected by a combination of a baseline and a rate effect (i.e. ASPs were affected in both young and old mice; the effect size was larger in old mice than in young mice). One possible interpretation is that age-dependent phenotypic change is in fact slowed in these cases (additionally to an age-independent effect on these ASPs). However, an alternative explanation is that shorter intervention exposure times in young mice account for smaller effects relative to old mice that were exposed to the intervention for a longer period. The shorter-term exposure to intermittent fasting in young mice (IF was initiated 4 weeks prior to the commencement of analyses), for instance, may have led to similar but smaller effects on some ASPs than the more long-term exposure (animals were on IF for 19 months prior to starting the analysis) in our aged cohort of animals. Future experiments should help distinguish between these scenarios by varying exposure time during a period in life where ASPs are relatively stable.

In our intervention studies, we examine cross-sectionally age-dependent changes in phenotypes between two time points (young adult vs. ca. 20 months old). As a consequence, our rate of change estimates refer to an overall change across this time period. A PAAI could potentially not only alter the rate of change but also modify the onset of age-dependent change (e.g., an intervention could lead to an earlier onset of change from baseline associated with a slower rate of change). We cannot address this possibility with our present dataset because that would require a study design with a number of age groups in between the young adult and aged group. Note though that rate of change estimates based on our two time points are well suited to measure the overall change on a population level that accumulates between young adulthood and 20 months of age.

We chose a large set of parameters for our analyses in mice to cover a broad range of age-related changes across numerous physiological systems and tissue contexts, spanning across multiple levels of biological organization (molecular, cellular, tissue, organismal). Our prior analyses established that a large and diverse number of ASPs can be captured using this approach^{10,16}. However, despite the comprehensive nature of our analysis it is important to note that our conclusions are based on the specific sets of parameters included in our assessment of age-related changes in mice. It will be important for the

field to complement our analyses with assessments of additional measures that extend the sets of ASPs included in the current study.

Our analyses were performed in a single genetic background (C57BL/6J) and one sex (male). It is currently unknown whether our observations extend to other genetic backgrounds and females.

In all our intervention studies, the aged groups of mice were ca. 20 months old when our analyses were started. Although this leaves unexamined older age groups with potentially additional aging-associated changes, we have chosen to examine 20-month old mice (and not older ones) to avoid interpretational issues that may arise from differential survival. For instance, if a longevity intervention does not improve age-sensitive phenotypes in 30-month old mice, this observation is difficult to interpret: Possibly, the intervention has truly no effects on age-sensitive phenotypes but, alternatively, differential survival could confound this analysis (e.g. controls with the poorest aging outcomes may have been eliminated from the population and, hence, cannot be analyzed, while mice with poor, but not yet detrimental aging outcome may still be existing in the intervention group, thereby resulting in a biased estimate of aging outcomes across these two populations). Assessing aged mice at 20 months largely eliminated differential survival as a confounding factor from our analysis (at 20 months, there has not yet been appreciable population attrition in the controls; see Fig. 1a), yet enabled us to measure and work with a large number of age-dependent changes in ASPs that are manifest in 20-month-old mice.

The determination of when aging begins to manifest is ultimately a matter of one's viewpoint and depends on the parameters one chooses to assess the consequences of aging⁹⁹. We applied a set of parameters that are relatively stable over at least some months in younger adult animals. If one intends to assess PAAIs in the context of parameters other than the ones used in the present study, it may be necessary to establish these parameters' individual lifetime profiles and to adjust the age of the young treated reference group, so that the PAAI can be restricted to a period prior to the onset of detectable age-dependent change.

Our conclusions are based on the specific set of PAAIs that were investigated in our current study (loss of function of *Ghrhr*, *mTOR*; intermittent fasting-based version of dietary restriction; see also Supplementary Discussion). As outlined above, our longevity mouse lines were chosen to represent important and central genetic/environmental lifespan-extending interventions established by prior research. *mTOR* signaling and growth hormone signaling are not only among the most well-established pathways in lifespan regulation^{9,16,24–55}, they also feature many links to cellular processes thought to generally play important roles in aging, such as proteostasis, nutrient sensing, inflammation and others^{4,71,100}. Similarly, dietary restriction regimens are thought to broadly influence a range of cellular processes linked to aging^{4,79}. Thus, our findings may have some generalizability beyond these three interventions. Nevertheless, how manipulations of other longevity-associated pathways interact with age-dependent change needs to be addressed in further studies examining additional genetic mutants and/or environmental manipulations. Note, however, that our study's implications potentially go well beyond the three specific PAAIs we examined: To the best of our knowledge, a convincing and broad (i.e., across a large set of ASPs) demonstration of effects on mammalian aging rate has, so far, not been provided for *any* PAAI (due to limits in scope and study design of prior work: Typically, only few ASPs are examined per study and the design does not allow to account for age-independent PAAI effects because young treated controls were not included).

A number of studies have applied multidimensional analytical approaches to measure organismal changes accompanying the aging process^{101–105}. An important feature of our study is that it uses multidimensional phenotypic data, covering multiple levels of complexity from molecular markers to complex physiological and tissue

functions, towards testing for a possible modulatory effect of genetic and environmental intervention effects on the aging process. Unlike studies in invertebrate models, our approach in mice captures mammalian physiology. In comparison to studies in humans, the experiments in mice facilitate causal and invasive experimentation (such as the genetic and fasting studies as well as the collection of many invasively obtained phenotypes that would be impossible to get in humans); they also facilitate the lifelong (or almost lifelong) exposure to experimental regimes (such as genetic and environmental manipulations that cover much of the organismal lifespan of a mouse).

Besides phenotypic analyses, we carried out transcriptome studies to test for age-dependent changes in tissue level gene expression. In addition to the full set of differentially expressed genes, we provide results derived from pathway analyses that were performed to detect whether specific pathways were enriched among the sets of differentially expressed genes. Note that the results for some of these annotated processes may seem counterintuitive, although they are expected. For instance, based on gene expression changes associated with advanced age, Ingenuity pathway analysis (IPA) derived predictions of reduced “organismal death” and “morbidity/mortality” in old mice. While these predictions appear to be inconsistent with the actually increased mortality rate associated with aging, they are expected¹⁰⁶ and are based on gene expression changes well known to be associated with aging (increased expression of inflammation-related genes in the context of aging¹⁰⁷) that lead IPA to predict a downregulation of the processes “organismal death” and “morbidity/mortality”. We also note that some of the IPA categories (such as many of the canonical pathways) contain a small number of member genes and/or may intersect with a small number of differentially expressed genes which can render these categories susceptible to variable results. These findings should not be over-interpreted without further study and corroboration.

Although there are few studies employing multi-point profiling of gene expression changes in rodent models, recent reports based on various rat and mouse tissues^{95,108}, indicated that most of the differentially expressed genes were first detectable during middle-ages (12–15 months) with progressive gradual changes till advanced age. However, there were notable differences across tissues, with the spleen for instance exhibiting more robust age-associated transcriptomic changes and in contrast, the brain being more resistant to aging⁹⁵. Moreover, pathway analysis of the differentially expressed genes associated with aging in these studies suggested the presence of both organ specific and global molecular signatures^{95,108}. These findings are consistent with our observations from spleen and brain bulk RNA-seq datasets (Fig. 2g–j, Supplementary Fig. 3).

In the present study, many age-sensitive phenotypes did not provide support for a slowing of age-dependent change in the PAAI groups, indicating that, in these cases, PAAIs did not exert their effects by inhibiting the accumulation of aging-associated damage. There are interesting parallels between these results and earlier observations: Dietary restriction (DR) in *Drosophila melanogaster* was found to reduce mortality risk entirely via short-term effects; flies that were transiently food-restricted and then switched to free access to food quickly adopted the mortality risk of flies that had free access to food throughout their lives¹⁰⁹, indicating that DR had no sustained influence on mortality risk (as one might expect if DR were to reduce mortality risk by slowing the accumulation of aging-associated damage).

Analyses of survival curves in pro-longevity mouse models indicated that the rate at which mortality risk increases with advancing age (captured in the Gompertz function parameter “G”) was unaffected¹¹⁰; instead, pro-longevity interventions in mice shifted the age at which mortality risk started to increase (captured in the Gompertz function parameter “A”) to older ages, without changing the rate of increase thereafter. Although it remains unclear how specifically these findings relate to ours, this observation has been interpreted as evidence that

changes in the “rate of aging” (based on a lack of effect on the parameter “G”) may not underlie the pro-longevity influences in mice, but rather changes in “baseline vulnerability” to adverse effects of disease and environmental factors (based on an effect on the parameter “A”) ¹¹⁰. In fact, resistance to the development of lethal neoplastic disease could represent such a change in “baseline vulnerability” in long-lived mutant mouse lines.

It is important to complement lifespan analyses with additional measures capturing age-dependent change, if one wishes to make statements about aging. This is particularly relevant in cases where it is unclear how well lifespan reflects broad changes across a range of physiological systems. In mice, for instance, lifespan is well known to be limited by the development of lethal neoplastic disease, indicating that it is determined by a rather narrow set of pathologies and hence cannot reflect aging-associated changes across a broader set of physiological systems^{5–10}. It will be an important task to further define the sets of biological processes that limit lifespan in other organisms, specifically in those that heavily informed the biology of aging via studies of lifespan (such as *C. elegans* and *D. melanogaster*)^{111–114}.

In the present work, we used age-dependent phenotypic change across a range of molecular, cellular, physiological and pathological markers as a proxy for biological aging. This does not imply that all aging-associated change is necessarily adverse. In fact, it has been pointed out that aging-associated alterations can have adaptive and beneficial effects for the aged organism^{115,116}. Future work will need to address which of the phenotypes employed in our present study design may serve adaptive purposes vs. may have detrimental effects for aging mice.

Aging is a multi-faceted process that transforms young adult into aged organisms. We believe that the identification of molecular regulators influencing aging will require approaches that measure many aspects of this organismal transformation directly, rather than relying on single or a small number of proxy markers. The isolated focus on lifespan, for instance, bears the risk of bias by putting center stage the subset of aging processes directly linked to lifespan (such as specific pathologies), but with potentially limited relevance for other facets of aging that do not per se determine the end of life. Much of what we currently think we know about molecular regulators of aging (summarized, e.g., in the “hallmarks of aging”⁴) has been derived from studies utilizing such proxy markers of aging. We therefore look forward to seeing more studies attempting to validate these regulators in the context of multidimensional phenotypic studies.

In conclusion, the PAAIs examined (i.e. *mTOR* loss of function, *Ghrhr* loss of function, intermittent fasting-based version of dietary restriction) often influenced age-sensitive traits in a direct way and not by slowing age-dependent change. Previous studies often failed to include young animals subjected to PAAI to account for age-independent PAAI effects. However, any study not accounting for such age-independent intervention effects will be prone to overestimate the extent to which an intervention delays the effects of aging on the phenotypes studied. This can result in a considerable bias of our view on how modifiable aging-related changes are. In the present study, we have covered considerable ground to address this important issue, focusing on non-preselected sets of phenotypes (non-preselected with regards to possible age or intervention effects) and analyzing three key longevity interventions in murine models. Our work indicates that these kinds of age-independent effects are common and identifies specific ASPs affected by such age-independent influences, which provides important insights for the reappraisal of the existing literature and the design of future studies.

Methods

Ethical statement

In accordance with the German Animal Welfare Act, the present study involving animals was approved by the “Landesamt für Natur, Umwelt

und Verbraucherschutz Nordrhein-Westfalen" (Recklinghausen, Germany) as well as the "Regierung von Oberbayern" (Munich, Germany). Approval to study trajectories of aging in human subjects was obtained from the ethics committee of the University of Bonn, Medical Faculty (Bonn, Germany). We obtained written informed consent from all participants in accordance with the Declaration of Helsinki.

Mice, age-sensitive parameters and interventions

We used wild-type C57BL/6J mice (Jackson Laboratory, Ben Harbor, ME, USA) to determine the trajectories of ASPs in mice. All the analyses described in the paper were restricted to male mice only. Animals for the quantification of ASP trajectories were assessed at 3, 5, 8, 14, 20 and 26 months of age: We had one cohort of mice for all deep phenotyping as well as RNA-seq analyses (data shown in Supplementary Data 1–5) and a separate cohort from which we harvested tissues for the molecular analyses presented in Supplementary Data 6. Three major longevity mouse lines were included in our analysis to address to what extent the corresponding interventions may or may not delay aging trajectories: These featured either a loss-of-function mutation in the *Ghrhr* gene (*Ghrhr*^{fl} mutation), were engineered to carry a hypomorphic *mTOR* mutant allele or were subjected to almost lifelong intermittent fasting. *Ghrhr*^{fl} mutants^{59,60}, also known as B6-little, were obtained from the Jackson Laboratory (stock no. 000533) (data summarized in Supplementary Data 7, 8 and 14). Founder animals of the hypomorphic *mTOR* mouse line⁵⁷, bearing a knock-in sequence replacing exon 12 within the murine *mTOR* gene, were kindly provided by Dr. Wendy DuBois (Laboratory of Cancer Biology and Genetics, Center for Cancer Research, National Cancer Institute, Bethesda, MD, USA) (data summarized in Supplementary Data 9–11, 15). After arrival at our facility, mice carrying the hypomorphic *mTOR* allele were crossed with wild-type C57BL/6J mice for five generations prior to use of the mice in the current analyses. The intermittent fasting (IF) cohort has been previously described and was generated using an every-other-day feeding paradigm in group-housed male wild-type C57BL/6J mice¹⁰ (current analysis summarized in Supplementary Data 12, 13, 16). In brief, intermittent fasting (IF) animals were subjected to alternating 24h-cycles of free access to food (Altromin 1314 standard rodent chow) and complete food deprivation, starting at the age of 8 weeks and continued throughout life of the animals. The Altromin 1314 chow came in solid pellets. Pilot experiments showed that mice did not crumble these pellets. Accordingly, removing the pellets on the restriction days was sufficient to fully deprive the animals of food (no cage change required). IF mice were compared to controls with *ad libitum* (AL) access to food throughout the course of the study. To evaluate whether these interventions' effects on ASPs are primarily due to either altering the rate of age-dependent change in ASPs or due to age-independent effects on ASPs, we analyzed aged mutant/fasted animals/wildtype littermate controls (if not stated otherwise, ~20 months old at the commencement of the deep phenotyping analysis) side-by-side with young mutant/fasted mice/wildtype littermate controls (~3 months old at the commencement of the deep phenotyping analysis).

Our deep phenotyping approach covered a wide range of analyses, including assessments of anatomical, physiological, metabolic, neuropsychiatric, cardiovascular, immunological, sensory, molecular, cellular and histopathological parameters. The following analyses were carried out in the order listed and were completed within a period of 11 weeks, if not stated otherwise^{17,118}: modified SHIRPA (week 1), open field (week 1), grip strength (week 1), rotarod (week 2), acoustic startle response and pre-pulse inhibition (week 2), clinical chemistry after fasting (week 3), hot plate test (week 4), body surface temperature (week 4), transepidermal water loss (week 4), indirect calorimetry (week 5), body composition analysis (week 5), glucose tolerance test (week 6), electrocardiography (week 7), echocardiography (week 7), Scheimpflug imaging (week 8), optical coherence tomography (week

8), laser interference biometry (week 8), virtual drum vision test (week 8), auditory brain stem response (week 9), bone densitometry (week 9), clinical chemistry (week 11), hematology (week 11), FACS-based analysis of blood leukocyte populations (week 11), immunoglobulins and plasma biomarkers (week 11), lymphocyte proliferation assay (week 11) and pathology (week 11). In general, animals, within their home cage, were allowed to habituate to the test room for a period of at least 15 min prior to the start of experimental procedures, if not stated otherwise. In all cases, experiments were carried out according to the IMPReSS (International Mouse Phenotyping Resource of Standardized Screens) workflow in compliance with the International Mouse Phenotyping Consortium (IMPC) (<https://www.mousephenotype.org/>) and the metadata was recorded. Analyses and procedures were always balanced across experimental groups. The number of animals examined depended on the specific experiment and assay used and is indicated in the data provided (for details, see Supplementary Data 2, 6, 8, 10, 13). Of note, assessments in IF mice were performed after a feeding day to avoid measuring acute hunger effects.

All mice were housed in individually ventilated cages (IVC) under specific pathogen-free conditions (according to FELASA guidelines) in groups of 2–5 mice. All mice were fed with Altromin 1314 standard rodent chow (composition: 5.1% fat (equivalent to 14% of total metabolizable energy), 22.5% protein (equivalent to 27% of total metabolizable energy) and 40.4% carbohydrates (equivalent to 59% of total metabolizable energy)). Husbandry conditions included a constant temperature of 22 °C, 55% humidity, a 12 h:12 h light/dark cycle as well as *ad libitum* access to food (except for IF animals as described above) and water. Local and federal regulations regarding animal welfare were followed. General welfare monitoring was performed on a daily basis. Prior to individual experiments, each animal was diligently checked for its suitability according to preset criteria approved by the local animal welfare authorities specified above. The animal was euthanized in case predefined humane endpoints, such as ulcerating tumor, bleeding from orifice or persistent rectal prolapse, were met. Sample size of mice cohorts were estimated using the G*Power software (v3.1.9.2) as required for ethical approvals of animal experiments.

Modified SHIRPA

The modified SHIRPA protocol was designed as a rapid semi-quantitative screen to detect phenotypic anomalies in mice¹¹⁹. Our SHIRPA test battery started with the inspection-based assessment of the animals' general appearance as well as their undisturbed behavior as observed in a transparent glass cylinder (11 cm in diameter). Mice were then transferred to a transparent Perspex box (420 mm × 260 mm × 180 mm), marked with a grid on the floor, for an assessment of general neurological status. A set of 17 tests were performed including assessments of the acoustic startle reflex, biting behavior, body position, contact righting reflex, defecation, gait, head bobbing, limb grasping, locomotor activity, pinna reflex, tail elevation, touch escape, transfer arousal, tremor, trunk curl, urination and vocalization.

Open field

To measure general locomotor activity in a novel environment, we subjected animals to an open field assay using a transparent and infrared light-permeable acrylic test box (45.5 cm × 45.5 cm × 39 cm inner dimensions) equipped with evenly spaced infrared light beams along the x- and y-axis and a rearing indicator covering the z-axis (ActiMot, TSE, Bad Homburg, Germany). Illumination in the center of the test box was set to ~200 lux; light intensity in the corners was ~150 lux. Animals were transferred to an area immediately adjacent to the test room where they were left undisturbed for a period of 30 min prior to commencement of open field analysis. In the open field

assay, mice were allowed to freely explore the novel environment (the open field box) for 20 min. Our analysis included the following parameters: distance traveled within the first 5 min, total distance traveled, number of rearings within the first 5 min, total number of rearings, percentage of distance traveled in the center of the box within the first 5 min, percentage of total distance traveled in the center of the box, percentage of the first 5 min spent in the center of the box, percentage of total time spent in the center of the box, average velocity.

Grip strength

Grip strength was measured using a grip strength meter system (Bioseb, Pinellas Park, FL, USA). The animal, held by its tail, was allowed to grab a metal grid with either two or four paws and was then pulled back horizontally. The maximum force applied to the grid, just prior to the animal losing grip, was recorded as the peak tension by a force sensor. Three trials were given to each mouse over the course of 1 min. Two-paw/four-paw grip strength was calculated by averaging the animals' performance over three consecutive trials.

Rotarod

Motor coordination and balance were evaluated on an accelerating rotarod (Bioseb, Pinellas Park, FL, USA)¹²⁰. After the mouse was placed on the apparatus, the rod was subjected to linear acceleration from 4 to 40 rpm over the course of the 5 min test period. The trial was terminated once the animal fell off the rod, displayed passive cycling or the 5 min time period had elapsed, whichever came first. Latency to fall was averaged across three trials given to each mouse with inter-trial intervals of 15 min.

Acoustic startle response and pre-pulse inhibition

Acoustic startle reflex and pre-pulse inhibition were assessed using a startle apparatus (Med Associates, Fairfax, VT, USA) equipped with four identical sound attenuating chambers (inner dimensions: 55.88 cm × 34.29 cm × 36.83 cm). Animals were left undisturbed in an area adjacent to the testing room for 30 min prior to the start of the experiment. Next, each mouse was habituated to the test compartment (a mouse restrainer) over a period of 5 min. Background noise was set to 65 dB. Bursts of white noise (40 ms in duration) were used as startle pulses. The protocol applied began with a 5 min acclimation period succeeded by five leader startle pulses at 110 dB that were excluded from analysis. Trial types for pre-pulse inhibition included four different pre-pulse intensities (67, 69, 73 and 81 dB) and generally preceded the startle pulse (110 dB) by 50 ms. Each trial type was presented 10 times in random order, organized in 10 blocks, each trial type occurring once per block.

Hot plate test

The hot plate test was carried out using an Analgesia Meter Hot Plate apparatus (TSE, Bad Homburg, Germany). In brief, the animal was placed on a metal surface maintained at 52 ± 0.2 °C which was surrounded by a cylindrical plexiglas restrainer (20 cm high, 18 cm diameter) in order to restrict movement of the animal. The trial was terminated once we observed one of three typical indications of pain (hind paw licking, hind paw shake/flutter or jumping); the mouse was then immediately removed from the metal plate. Latencies and response type (hind paw licking, hind paw shake/flutter or jumping) were recorded. The maximum duration of this test was limited to 30 s in order to avoid tissue damage.

Body surface temperature

Body surface temperature was assessed using infrared thermovision. Specifically, we determined maximal, average and minimal body surface temperature using a FLIR A655sc camera system (FLIR Systems, Wilsonville, OR, USA).

Transepidermal water loss

Transepidermal water loss via diffusion or evaporation was assessed non-invasively with an AquaFlux AF200 evaporimeter (Biox Systems, London, UK). To quantify the amount of transepidermal water loss, the probe was placed on the skin of the mouse for a period of 60–90 s.

Indirect calorimetry

Metabolic turnover was analyzed via indirect calorimetry. Mice were single-housed in individually ventilated metabolic cages (PhenoMaster, TSE, Bad Homburg, Germany) at 23 °C and were maintained on a 12 h:12 h light dark cycle (lights on at 6 am, light off at 6 pm). Metabolic cages were constantly supplied with fresh air and changes in O₂ and CO₂ levels were recorded by high precision sensors in every cage. Additionally, locomotion and rearing activity were detected by infrared sensors surrounding the cages. Animals were habituated to the metabolic cages for a period of 2 h prior to starting measurements. Recordings were generally carried out over a period of 24 h, except for the study of IF mice in which we measured for 47 h to accommodate metabolic analyses during both feeding and fasting days. All mice were granted free access to food and water with the exception of IF mice which were only fed during the first 24 h. Relevant parameters determined by indirect calorimetry included minimal O₂ consumption, average O₂ consumption, maximal O₂ consumption, minimal respiratory exchange rate (RER, computed as volume of CO₂ generated (VCO₂)/volume of O₂ consumed (VO₂)), average RER, maximal RER, ΔRER (maximal RER – minimal RER), minimal heat production (calculated using the formula: heat production (mW) = (4.44 + 1.43 × RER) × VO₂ (ml/h)), average heat production, maximal heat production, cumulative food intake, cumulative water consumption, total distance traveled, cumulative number of rearings and cumulative number of fine movements. In addition, body weight was measured at the beginning and at the end of the metabolic assessments.

Body composition analysis

Time Domain Nuclear Magnetic Resonance (TD-NMR)-based body composition analysis was carried out by placing animals into a Minispec Whole Body Composition Analyzer (Bruker, Billerica, MA, USA). Measures of interest were lean mass, fat mass, and total amount of free body fluid.

Glucose tolerance test

We carried out an intraperitoneal glucose tolerance test (IpGTT) subsequent to six hours of food deprivation. Body weight was recorded before and after the fasting period. The tip of the tail was scored and a small drop of blood was used to determine the base glucose level via an Accu-Chek Aviva glucose analyzer (Roche, Basel, Switzerland). After 2 g glucose per kg body weight was injected intraperitoneally, blood glucose levels were sequentially measured at four additional time points (15, 30, 60 and 120 min after injection).

Electrocardiography

Non-invasive electrocardiographs (ECG) were recorded using ECGenie (Mouse Specifics, Framingham, MA, USA) in conscious animals¹²¹ in order to avoid effects of anesthesia on cardiac function¹²². Cardiac electrical activity was measured through the paws of the animal staying on a shielded acquisition platform. Intervals and amplitude from at least 15 consecutive ECGs were averaged. Heart rate was calculated from peak detections. P, Q, R, S and T waves were analyzed such that unfiltered noise or motion artifacts were excluded. The corrected QT interval (QTc) was calculated by dividing the QT interval by the square root of the preceding RR interval. QT dispersion represents inter-lead variability between QT intervals. QTc dispersion was calculated as the rate QTc dispersion. Relevant parameters included were: duration of the P wave, PR interval, QRS interval, QT interval, QT dispersion, QTc, QTc dispersion and RR interval.

Echocardiography

We performed transthoracic echocardiography in awake animals using the Vevo 2100 Imaging System (Visual Sonics, Toronto, Canada) equipped with a 30 MHz transducer. Anatomic structure and cardiac function of the left ventricle were analyzed by dual mode imaging. Specifically, left ventricular parasternal short- and long-axis views were imaged in B-mode and left ventricular parasternal short-axis imaging was performed in M-mode at the papillary muscle level. Short-axis M-mode images derived from three consecutive heart beats were used to measure the following anatomic parameters: left ventricular end-diastolic internal diameter (LVIDd), left ventricular end-systolic internal diameter (LVIDs), diastolic septal wall thickness (IVSd), systolic septal wall thickness (IVSs), thickness of the left ventricle posterior wall during diastole (LVPWd) and thickness of the left ventricle posterior wall during systole (LVPWs). Corrected mass of the left ventricle (LV mass corr) was computed as $LV\ mass\ corr = 0.8 \times (1.053 \times ((LVIDd + LVPWd + IVSd)^3 - LVIDd^3))$. Additionally, we determined ejection fraction (ES), fractional shortening (FS) as well as stroke volume (SV). EF was calculated as $EF\% = 100 \times ((LVvolD - LVvolS)/LVvolD)$ with $LVvol = ((7.0/(2.4 + LVID) \times LVID^3)$. The formula $FS\% = ((LVIDd - LVIDs)/LVIDd) \times 100$ was used to calculate FS. The difference between the end-diastolic and the end-systolic blood volumes during one heartbeat was defined as SV. We also measured heart and respiration rates during echocardiographic assessment.

Scheimpflug imaging

Optical density and morphology of lens as well as cornea were assessed in a contact-free manner using the Pentacam system (Oculus, Wetzlar, Germany). For the acquisition phase, the mouse was placed on a platform in front of the apparatus and the eye was positioned towards a vertical light source (LEDs, 475 nm). The distance between eye and the Pentacam device was adjusted automatically by the software to gain optimal focus.

Optical coherence tomography

The posterior segment of the eye, including retina and fundus, were evaluated in anaesthetized mice using a Spectralis OCT device (Heidelberg Engineering, Heidelberg, Germany). After 1% atropine was administered to widen the pupils, a small amount of Methocel 2% (OmniVision, Puchheim, Germany) was used to carefully place a contact lens of 10 mm focal length (Roland Consult, Brandenburg an der Havel, Germany) onto the eye. For measurements, the animal was placed on an elevated platform in order to optimally position the eye in front of the transducer of the recording unit. Images were taken as described previously¹²³. We measured thickness and morphology of the retina, as well as morphology of the optical disk, fundus pigmentation and the number of main blood vessels.

Laser interference biometry

Eye size measurements were performed using the AC Master system (Carl Zeiss Meditec, Jena, Germany). Briefly, anaesthetized mice were placed on a platform. Proper positioning of the animals was supported by light signals from six infrared LEDs arranged in a circle that must be placed in the center of the pupil. Eyes were treated with 1% atropine to ensure pupil dilation. Central measurements of axial eye length were performed as described elsewhere¹²⁴.

Virtual drum vision test

Visual acuity was tested using OptoMotry, a virtual optomotor system (Cerebral Mechanics, Westchester County, New York, USA) as described previously¹²⁵. Prior to the start of the assessments, animals were placed on an elevated platform surrounded by four computer monitors. Animals were then allowed to track a virtual rotating cylinder comprised of a sine wave grating and their movements were recorded by an overhead camera. A lack of compensatory head and neck

movements countering the motion of the sine wave grating indicates an inability to discern the displayed visual pattern. Rotation speed and contrast of this test was set to 12 d/s and 100%, respectively.

Auditory brain stem response

Non-invasive assessments of hearing sensitivity were performed using an auditory brain stem response (ABR) test (Industrial Acoustics Company, North Aurora, IL, USA). After anaesthetizing the animals via i.p. injection of a ketamine/xylazine mixture, mice were placed on a heated blanket (37–38 °C) and were then transferred to the acoustic chamber. Subsequently, three electrodes were placed subcutaneously (COM-electrode behind the right ear, G1-electrode on top of the skull and G2-electrode underneath the left ear). Auditory brain stem responses were induced using different acoustic stimuli, including clicks of 0.01 ms duration and beeps of a given frequency (6, 12, 18, 24 and 30 kHz; 5 ms duration, 1 ms rise/fall time). Hearing threshold levels for the respective stimuli were determined by gradually elevating sound intensity from 5 to 85 dB SPL in 5 dB steps.

Bone densitometry

Bone densitometry was performed non-invasively using either dual-energy X-ray absorptiometry (DXA) or micro-CT imaging in anesthetized animals. DXA analyses were performed using an UltraFocus DXA system (Faxitron Bioptics, LLC, Tucson, AZ, USA). Relevant parameters examined included bone area, bone mineral content, bone mineral density and volumetric bone mineral density of the whole animal excluding the skull. Micro-CT analysis of tibiae of IF mice and their controls was processed using a SkyScan 1172 micro-CT scanner (Bruker, Billerica, MA, USA). A resolution of 7.88 μm pixel was achieved at 80 kV voltage, 100 mA current and using a 0.5 mm aluminum filter. Images acquired from cross-sectional slices of the distal tibia (197 μm from 25 slices halfway between the tibia-fibula junction and the distal end of the tibia) were reconstructed by the SkyScan volumetric NRecon reconstruction software (v1.7.5.0) (Bruker, Billerica, MA, USA) and further analysis was performed using the CT Analyser software (CTAn, v1.15) (Bruker, Billerica, MA, USA). Relevant parameters were: total tissue area, bone area, marrow area, cortical thickness and polar moment of inertia.

Blood sampling

For blood sample collection, the animals' retrobulbar sinus was punctured using non-heparinized glass capillaries (1 mm diameter) after inducing anesthesia with isoflurane. To assess metabolic parameters in the fasted state, blood specimens were collected in heparinized tubes from animals after an overnight 16-h food withdrawal. Blood collected from animals in the fed state were distributed into three portions. While the larger fraction was collected in heparinized tubes, we also collected two portions in EDTA-coated tubes. To ensure homogeneous distribution of the anticoagulant, tubes were inverted five times after blood collection. Samples were then stored at room temperature for 1–2 h. Next, heparinized tubes were centrifuged for 10 min at 4 °C and 4200 g to pellet the blood cells for the collection of plasma. Plasma from the heparinized blood samples were used in part for the immunoglobulin and plasma biomarker measurements. Another fraction was used for clinical chemistry-based measures in the fasted and fed state. Hematological analyses were performed using one portion of EDTA blood samples derived from animals in the fed state. Another portion of EDTA blood samples was used for FACS-based quantification of leukocyte populations.

Clinical chemistry

Assessments of clinical chemistry parameters were performed using an AU480 Automated Chemistry Analyzer (Beckman Coulter, Brea, CA, USA) and specific kits for free fatty acids (Wako Chemicals, Neuss, Germany), glycerol (Randox Laboratories, Crumlin, UK) as well as all

other parameters covered by the present study (Beckman Coulter, Brea, CA, USA)¹²⁶. A set of 21 parameters consisting of specific metabolite levels, electrolyte concentrations and enzyme activities was measured in fed mice: albumin, α -amylase, alkaline phosphatase (AP), aspartate-aminotransferase (ASAT/GOT), alanine-aminotransferase (ALAT/GPT), calcium, cholesterol, chloride, creatinine, fructosamine, glucose, iron, lactate, lactate dehydrogenase (LDH), phosphate, potassium, sodium, total protein, triglycerides, urea and unsaturated iron-binding capacity. In addition, a selection of parameters (cholesterol, glucose, glycerol, HDL-cholesterol, non-esterified fatty acids (NEFA), non-HDL cholesterol and triglycerides) was measured in fasted animals after 4 (Ghrhr study), 6 (IF study) or 16–18 h (mTOR study, C57BL/6j baseline study) of food deprivation. Plasma insulin levels were measured using a commercial kit based on immunoelectrofluorescence (Mesoscale Discovery, Rockville, Maryland, USA) or ELISA technology (Merckodia, Uppsala, Sweden).

Hematology

EDTA-blood samples were diluted 1:5 in Sysmex Cell-Pack buffer (Sysmex, Kobe, Japan) prior to performing blood cell counts via a Sysmex XT2000iV device (Sysmex, Kobe, Japan). Parameters analyzed included red blood cell count (RBC), hematocrit (HCT), hemoglobin concentration (HBG), mean corpuscular hemoglobin content (MCH), mean corpuscular hemoglobin concentration (MCHC), mean corpuscular volume (MCV), red blood cell width distribution (RDW), platelet count (PLT), mean platelet volume (MPV), platelet distribution width (PDW), platelet large cell ratio (PLCR, >12 fl) and total white blood cell count (WBC).

FACS-based analysis of peripheral blood leukocytes

Whole blood samples were incubated with Fc block (clone 2.4G2) for 5 min at 4–10 °C. Subsequently, blood leukocytes were stained using a mixture of fluorescence-conjugated monoclonal antibodies (BD Biosciences, Franklin Lakes, NJ, USA) for 1 h at 4–10 °C. After lysis of erythrocytes and a formalin-based fixation, samples were analyzed using a Gallios ten-color flow cytometer (Beckman Coulter, Brea, CA, USA) combined with an IntelliCyt HyperCyt sampler (Sartorius, Göttingen, Germany). The acquisition threshold (trigger) was set on the CD45-channel¹²⁷. A total number of 10,000–50,000 leukocytes per sample was examined. Frequencies of leukocyte populations were determined by software-based analysis (Flowjo, v10.8.1, TreeStar Inc, USA; and SPICE¹²⁸). Gates for each parameter were based on formerly performed ‘fluorescence minus one’ (FMO) controls¹²⁹. Surface antigens used to define leukocyte populations were: B220, CD3, CD4, CD5, CD8, CD11b, CD11c, CD19, CD25, CD44, CD62L, Ly6C, Ly6G, NK1.1, NKp46 and gamma delta T cell receptor (gdTCR). Detailed information regarding the definition of relevant cell subpopulations and gating strategies applied is provided in Supplementary Data 2 as well as Supplementary Figs. 18, 19. The list of antibodies applied is provided in Supplementary Table 1.

Analysis of cytokine and immunoglobulin abundance in plasma samples

The abundance of several plasma biomarkers was determined using MULTI-ARRAY technology MSD (Meso Scale Discovery, Rockville, MD, USA). MSD-Mouse Isotyping Panel (IgA, IgM, IgG1, IgG2a, IgG2b, IgG3), MSD-Mouse Proinflammatory Panel (IFN- γ , IL-1 β , IL-2, IL-4, IL-5, IL-6, IL-10, IL-12p70, KC/GRO) and MSD-U-PLEX Custom (IgE, Insulin, IL-6, and TNF- α) were quantified side by side on MULTI-SPOT plates.

Lymphocyte proliferation assay

For monitoring T and B cell proliferation rates, single cell suspensions were prepared from spleens of mice at different ages. Cells were then stimulated *in vitro* as described below. Assessment of Class Switch Recombination was performed using stimulation with a mixture of

anti-CD40 antibody (Thermo Fisher Scientific, Waltham, MA, USA) and IL-4 (Thermo Fisher Scientific, Waltham, MA, USA) (applied at concentrations of either 1 μ g/ml anti-CD40 + 5 ng/ml IL-4 or 5 μ g/ml anti-CD40 + 10 ng/ml IL-4) followed by a cultivation period of 7 days. For the assessment of T cell proliferation, cells were treated with a mixture of anti-CD3 antibody (Thermo Fisher Scientific, Waltham, MA, USA) and IL-2 (Thermo Fisher Scientific, Waltham, MA, USA) (at 1 μ g/ml anti-CD3 + 1 ng/ml IL2 or 5 μ g/ml anti-CD3 + 10 ng/ml IL-2) followed by cultivation for 3 days. The CellTiter-Glo Luminescent Cell Viability Assay kit (Promega, Madison, WI, USA) was used for proliferation measurements following the manufacturer’s instructions. The luminescence signal was read using a Microplate Reader (Tecan Infinite M200; Tecan, Männedorf, Switzerland). Detailed information regarding antibodies applied is provided in Supplementary Table 1.

Pathology

During necropsy, mice were examined morphologically. Body and organ weights/length measurements as well as any tissue lesions were documented by experienced necropsy technical personnel using an annotation approach developed for high-throughput mouse phenotyping (<https://www.mousephenotype.org/impress/procedures/14>). The following organs were collected, fixed in 4 % neutral buffered formalin and embedded in paraffin: abdominal aorta, adipose tissue (brown and white), adrenal gland, brain, bone (femur), epididymis, heart, intestine, kidney, liver, lung, pancreas, reproductive organs, skeletal muscle, skin, spleen, stomach, thymus, thyroid gland and urinary bladder. For histological examination, we generated 2- μ m sections from the respective organ samples and stained them with either Haematoxylin-Eosin (HE), Periodic Acid Schiff (PAS), Van Gieson or Movat Pentachrome. Digital scans of stained slides were processed using a NanoZoomer HT2.0 slide scanning system (Hamamatsu Photonics, Hamamatsu, Japan) and were analyzed by two experienced pathologists.

Organ harvest and processing for molecular analyses

After animals were sacrificed with CO₂, organs (brain, lung and spleen) were harvested quickly, snap-frozen in liquid nitrogen and stored at –80 °C. Frozen tissue samples were then pulverized in liquid nitrogen using a porcelain mortar and pestle (MTC Haldenwanger, Waldkraiburg, Germany) maintained on dry ice. Several aliquots of tissue powder were made and stored at –80 °C until further use.

RNA extraction, RNA-seq and data processing

Total RNA isolation from mouse tissues was performed with TRI-Reagent (Merck, Darmstadt, Germany). Briefly, 1 ml TRI-Reagent was added to an aliquot of frozen tissue powder followed by solubilization via ten passages through a 24-gauge needle. Further processing steps were performed according to the manufacturer’s recommendations. Total RNA was purified with the Monarch RNA Cleanup kit (New England Biolabs, Ipswich, MA, USA).

A previously described protocol¹³⁰ was used for mRNA isolation and cDNA library preparation with a few modifications. Briefly, mRNA was isolated from purified 1 μ g total RNA using oligo-dT beads (New England Biolabs, Ipswich, MA, USA) and fragmented in reverse transcription buffer by incubating at 85 °C for 7 min, before cooling on ice. SmartScribe reverse transcriptase (Taraka Bio, Kusatsu, Japan) with a random hexamer oligo (HZG883: CCTTGGCACCCGAGAATTCCANNNNN) was used for cDNA synthesis. Samples were then treated with RNase A and RNase H to remove RNA, followed by purification of cDNA on Agencourt AMPure XP beads (Beckman Coulter, Brea, CA, USA). The single stranded cDNA was ligated with a partial Illumina 5’ adapter (HZG885: 5phos/AGATCGAAGAGCGTCGTAGGGAAGAGTGT ddC) using T4 RNA ligase 1 (New England Biolabs, Ipswich, MA, USA) and incubated overnight at 22 °C. Ligated cDNA was purified on AMPure XP beads and amplified by 20 cycles of PCR using FailSafe PCR

enzyme (Epicenter Technologies, Thane, India) and oligos that contain full Illumina adapters (LC056: AATGATACGGCGACCACCGAGATCTACACTCTTTCCCTACACGACGCTCTTCCGATCT and unique index primers: CAAGCAGAAGACGGCATACGAGATnnnnnnnnnGTGACTGGAGTTCCTTGGCACCCGAGAATTCCA, where nnnnnnnnn indicates index nucleotides) for each sample. The resulting cDNA libraries were purified on AMPure XP beads, size selected using SPRIselect beads (Beckman Coulter, Brea, CA, USA), and quantified by Qubit dsDNA HS Assay Kit (Thermo Fisher Scientific, Waltham, MA, USA) prior to pooling. The pooled library was run on an Agilent High Sensitivity DNA chip (Agilent Technologies, Santa Clara, CA, USA) with an Agilent 2100 Bioanalyzer instrument (Agilent Technologies, Santa Clara, CA, USA) to check the quality and average fragment size.

Pooled indexed cDNA libraries were sequenced on an Illumina NovaSeq 6000 system (Illumina, San Diego, CA, USA) with a single 111 bp read and 10 bp index read. Demultiplexing and data transformation to generate fastq files was done using bcl2fastq2 (v2.20). Sequencing reads were trimmed using CutAdapt (<https://usegalaxy.org/>) to remove adapter sequences. Trimmed reads were mapped to the mouse transcriptome (GRCm38, mm10) using HISAT2 (v2.1.0) in Galaxy (<https://usegalaxy.org/>) with forward strand information and default settings. Bam files were indexed using Samtools and count matrices generated by Genomic Alignments in R. Gene count matrices were generated using annotation information from a *Mus musculus.GRCm38.102.chr.gtf* file imported with the rtracklayer³¹ package into R. All downstream analyses were performed using R (Version 3.5.1, <https://cran.r-project.org/>). Library normalization and expression differences between samples were quantified using the DESeq2 package³². A false discovery rate (FDR) < 0.05 was used as a cutoff in differential expression analyses. Assessment of the significance of the overlap of mTOR- and age-sensitive genes was performed based on exact hypergeometric probability.

Sample sizes for RNA-seq analyses were as follows: 3 months, $n = 7$ mice; 5 months, $n = 9$ mice; 8 months, $n = 8$ mice; 14 months, $n = 9$ mice; 20 months, $n = 7$ mice; 26 months, $n = 5$ mice (Supplementary Data 3, 4); young/old mTOR mutant mice and WT littermate controls, each $n = 3$ mice per group (Supplementary Data 11).

Real-time quantitative PCR

Total RNA was reverse-transcribed by the iScript cDNA Synthesis Kit (Bio-Rad Laboratories, Hercules, CA, USA). Real-time quantitative PCR based on the SYBR Green method was performed using the PowerUP SYBR Green Master Mix (Thermo Fisher Scientific, Waltham, MA, USA) on a StepOnePlus Real-Time PCR System (Thermo Fisher Scientific, Waltham, MA, USA). The threshold cycle value (Ct) of each target gene was normalized to the corresponding Ct value of β -actin (*Actb*). Primer sequences used are provided in Supplementary Table 3.

Protein isolation

To generate tissue homogenates suitable for measuring levels of lipid peroxidation, 20S proteasome activity as well as reactive oxygen species production, 300 μ l Tris-Buffered Saline (TBS, pH 7.6) and 1% Triton X-100 (Merck, Darmstadt, Germany) were added to a tissue powder aliquot and homogenization was performed using ten consecutive passages through a 24-gauge needle on ice. After a 30 min incubation step on ice, samples were centrifuged at 15000 \times g for 30 min at 4 °C. The supernatant was aliquoted into new tubes and stored at -80 °C until use. To generate protein homogenates suitable for western blot analysis, 300 μ l Tris-Buffered Saline (TBS, pH 7.6) + 1% Triton X-100 (Merck, Darmstadt, Germany) supplemented with 1x Protease Inhibitor Cocktail (Roche, Basel, Switzerland) and 1x PhosSTOP Phosphatase Inhibitor Cocktail (Roche, Basel, Switzerland) was added to a tissue powder aliquot. Further processing steps were analogous to the ones described above.

Lipid peroxidation

Levels of thiobarbituric acid reactive substances (TBARS), a byproduct of lipid peroxidation, were determined using a TBARS Assay Kit (Cayman Chemical, Ann Arbor, MI, USA) following the manufacturer's instructions.

Proteasome activity

The 20S proteasome activity was assessed in vitro using a protocol published elsewhere³³. Developing buffer (50 mM Tris (pH7.5), 150 mM NaCl, 5 mM MgCl₂) containing 30 μ g protein in a total volume of 94 μ l was loaded onto a black 96-well plate (Sarstedt, Nümbrecht, Germany). Two μ l 50 mM ATP-Mg²⁺ (Merck, Darmstadt, Germany), 2 μ l 5 mM Suc-LLVY-AMC substrate (Cayman Chemical, Ann Arbor, MI, USA) and 2 μ l 1% SDS (Carl Roth, Karlsruhe, Germany) were added immediately prior to commencing the experiment. Reaction suspensions were incubated in the dark at 37 °C for 30 min and fluorescent signals (excitation 380 nm, emission 460 nm) were acquired using a Tecan Infinite M200 Pro plate reader (Tecan, Männedorf, Switzerland).

Reactive oxygen species

Production of reactive oxygen species (ROS) in mouse tissues was measured in vitro using a previously described protocol³⁴ with a few modifications. All chemicals used in this assay were purchased from Merck (Darmstadt, Germany). We mixed 45 μ l protein samples (30 μ g protein) with 50 μ l ice-cold 2x Locke's buffer (308 mM NaCl, 11.2 mM KCl, 7.2 mM NaHCO₃, 4 mM CaCl₂, 20 mM D-glucose, 10 mM HEPES (pH7.4)) and loaded this mixture onto a black 96-well plate (Sarstedt, Nümbrecht, Germany). We then added 5 μ l 200 μ M 2',7'-dichlorodihydrofluorescein diacetate (DCFH-DA) and the reaction mixture was incubated in the dark on an orbital shaker for 30 min at room temperature and 50 rpm. Fluorescent intensities (excitation 485 nm, emission 530 nm) were acquired using a Tecan Infinite M200 Pro plate reader (Tecan, Männedorf, Switzerland).

DNA damage

Quantification of 8-hydroxy-2'-deoxyguanosine was performed using the DNA Damage Competitive ELISA Kit (Thermo Fisher Scientific, Waltham, MA, USA) following the manufacturer's instructions.

Western blot

All chemicals and reagents used in this procedure were purchased from Merck (Darmstadt, Germany), if not specified otherwise. We mixed 30 mg protein samples with the appropriate amount of 4x loading buffer (240 mM Tris-HCl (pH 6.8), 8% SDS, 5% beta-mercaptoethanol, 40% glycerol and 0.04% bromophenolblue) and ran this mixture through handcast Tris-glycine gels prior to blotting onto nitrocellulose membranes with 0.1 μ m pore size (GE Healthcare, Chicago, IL, USA). Subsequently, the membranes were incubated with Phosphate-Buffered Saline (PBS) + 10% skim milk powder for 1 h at room temperature to reduce background noise. Primary antibody solutions, diluted in PBS + 1% milk, were applied overnight at 4 °C. A detailed list of primary antibodies used is provided in Supplementary Table 4. Secondary antibodies, either goat anti-rabbit (Promega, Madison, WI, USA) at 1:3000 dilution or goat anti-mouse (Agilent Technologies, Santa Clara, CA, USA) at 1:10000 dilution, were used at room temperature with an incubation time of 90 min. Immunoreactivity was visualized via enhanced chemiluminescence (Advansta, Menlo Park, CA, USA) and band densities were quantified using ImageJ software (version 1.50e, National Institute of Health, USA). Phosphorylated proteins were normalized to the respective total protein band on the same lane. In all other cases, normalization was carried out using the Actin signal derived from the same lane. Whenever multiple protein targets were determined on the same membrane, signals derived from preceding visualizations were erased by adding a sodium azide incubation step in between protein target measurements.

Aging-related (endo)phenotypes in humans

The human data were collected in the context of the Rhineland Study, which is an ongoing, large-scale, single-center, population-based prospective cohort study among people aged 30 years and above in Bonn, Germany. The only exclusion criterion is insufficient command of the German language to provide informed consent. Persons living in the recruitment areas are predominantly German from Caucasian descent. One of the Rhineland Study's primary objectives is to identify determinants and markers of healthy aging, utilizing a deep-phenotyping approach. Participants of the Rhineland Study don't receive any monetary compensation.

For these analyses, we used baseline data of the first 3034 participants of the Rhineland Study who had both phenotype and genotype data available. Fifty-four aging-related (endo)phenotypes representing ten physiological functional domains, including body composition (5 phenotypes), body fat distribution based on magnetic resonance imaging (MRI) (4 phenotypes), cardiology (7 phenotypes), clinical chemistry (11 phenotypes), hematology (9 phenotypes), inflammation (4 phenotypes), immunology (6 phenotypes), muscle strength (2 phenotypes), ophthalmology (2 phenotypes) and physical activity (4 phenotypes), were included. Further details of the study have been described previously^{61,135,136}

Statistics and data analysis

Phenotypic and molecular data were analyzed across age groups using one-way ANOVAs with the between-subjects factor age, followed by Fisher's LSD posthoc analyses if appropriate (using base R version 3.6.1 and the package 'agricolae' version 1.3-1). We analyzed non-parametric data across age-groups using Kruskal–Wallis tests, followed by Dunn tests where appropriate (using base R version 3.6.1 and the package 'FSA' version 0.8.26). Count-based data (histopathology) were analyzed using Fisher's exact test across all age groups, followed by pairwise comparisons against the 3 months old reference group if appropriate (using base R version 3.6.1 and the package 'rcompanion' version 2.3.7). Throughout the manuscript, we report two-tailed *p*-values. Age-sensitivity of parameters was determined by evaluating the *p*-value ($p < 0.05$) of the global comparison (i.e., ANOVA, Kruskal–Wallis or Fisher's exact test). The age at first detected phenotypic change was determined by assessing the results of the posthoc tests vs. the 3 months old reference group. For instance, we considered a phenotype to be age-sensitive and to feature an age at first detected change of 8 months if the global test (i.e., ANOVA, Kruskal–Wallis or Fisher's exact test) for an age effect was significant ($p < 0.05$) and the posthoc analyses vs. the 3 months old group were not significant for the comparison 3 vs. 5 months, but significant for all other tests (3 vs. 8, 3 vs. 14, 3 vs. 20, 3 vs. 26) with the maximum possible exception of one comparison. For PCA of phenotypic data, all continuous variables available were included in the analysis. PCA was performed using base R version 3.6.1 and the packages 'FactoMineR' (version 2.0) and 'factoextra' (version 1.0.6). Multivariate imputation by chained equations was used for imputation in case of missing values (using base R version 3.6.1 and the package 'mice' version 3.13.0).

Phenotypic data from our intervention studies (*mTOR*, *Ghrhr*, IF) were analyzed using two-way ANOVAs with the between-subjects factors age and intervention (genotype or diet). We used a full ANOVA model, including an intervention \times age interaction term. These analyses were followed by Fisher's LSD posthoc tests where appropriate (using base R version 3.6.1 and the package 'agricolae' version 1.3-1). Non-parametric data (SHIRPA outcomes, data from auditory brain stem responses) were analyzed using Aligned Rank Transform with the factors age and intervention (including an intervention \times age interaction term), followed by Mann–Whitney U tests for posthoc analyses if appropriate (using base R version 3.6.1 and the package 'ARTool' version 0.10.6). Count-based data (histopathology) were analyzed using

Fisher's exact test across age and intervention groups, followed by pairwise comparisons if appropriate (using base R version 3.6.1 and the package 'rcompanion' version 2.3.7). We visualized the relationship of age and intervention effects using Venn diagrams (shown in panels c of Figs. 3–5). These show the numbers of age-sensitive phenotypes (parameters with a main effect of age, $p < 0.05$), genotype/diet-sensitive phenotypes (parameters with a main effect of genotype/diet), the number of parameters with a significant genotype/diet \times age interaction ($p < 0.05$), as well as the intersection between these parameter sets. Standardized coefficients with 95% confidence intervals, corresponding to the age effects, intervention effects and intervention \times age interactions, derived from linear models applied to all continuously distributed phenotypes included in the present study, are presented in Supplementary Fig. 6. Sunburst diagrams in panels c of Figs. 3–5 focus on all age-sensitive phenotypes (ASPs) shown in the Venn diagram and dissect these into ASPs not influenced by genotype/diet, ASP accentuated by genotype/diet and ASP ameliorated by genotype/diet. To address whether age-sensitive phenotypes in the intersection (associated with both age and diet) are ameliorated or accentuated by the intervention (genotype/diet) we evaluated effect sizes (Cohen's *d*; computed using the R package *effsize* version 0.7.6) of age, as well as intervention in the old group: If Cohen's *d* values pointed in the same direction, ASPs were considered to be accentuated, if they were in opposing directions, ASPs were considered to be ameliorated by the intervention. ASPs were not considered in cases where Cohen's *d* values could not be computed (because of 0 values in the denominator). For ASPs ameliorated by genotype/diet, the sunburst diagrams also provide the proportion of ASPs influenced via either a genotype/diet main effect and/or via a genotype/diet \times age interaction (inner ring of the sunburst diagrams). The outer ring of the sunburst diagrams shows the proportional distribution of the age at first detected phenotypic change of ASPs (based on the parameters for which this information had been collected in the context of our aging trajectories baseline study). We used an analogous approach for the analysis of gene expression data: In this case, the Venn diagram shows the number of age-sensitive genes (genes with a main effect of age, $FDR < 0.05$), genotype-sensitive genes (genes with a main effect of genotype, $FDR < 0.05$), genes with a significant genotype \times age interaction ($FDR < 0.05$), as well as the intersection between these parameter sets. Instead of Cohen's *d* values, we used log₂ fold changes for the comparisons of age and genotype effects but otherwise the proceeding was analogous to the approach used for the assessment of phenotypic data described above. Linear regression analyses of effect size estimates were carried out using GraphPad Prism version 8 (La Jolla, CA, USA). We performed intraclass correlation analyses using base R version 3.6.1 and the package 'psych' (version 2.0.7). Statistical comparison of Cohen's *d* effect sizes for individual phenotypes was carried out as described in⁷⁸ (for further details, see also our analysis code available at https://github.com/ehningerd/Xie_et_al-longevity_regulators).

For the statistical analyses in humans, characteristics of the study participants were reported as means (standard deviations (SD) and ranges) for continuous variables and numbers and percentages for categorical variables. The eQTL dosage was coded as GG = 0, AG = 1, and AA = 2 for *GHRHR*, and as GG = 0, CG = 1, and CC = 2 for *MTOR*. All variables representing (endo)phenotypes were standardized before further analyses in order to enable better comparison of the effect sizes across different physiological and functional domains. Given the low rate of missingness (<5%), all analyses were based on cases with complete data. Multiple linear regression analyses were applied to quantify the association between eQTL dosage (determinant) and each (endo)phenotypic measure (outcome). Models were adjusted for age, sex and population stratification using the first ten genetic principal components. In addition, inflammation markers were adjusted for batch information, MRI-based fat measurements were adjusted for

height of the segmented region as described previously^{61,135,136}, and physical activity variables were adjusted for examination season and the number of valid recoding days. For (endo)phenotypes where a *GHRHR*- and/or an *MTOR*-genotype effect was observed, we further assessed the interaction between age and each eQTL to evaluate age-(in)dependency of the effect estimates. All standardized effect estimates are reported together with their 95% confidence intervals (CIs).

Statistical analyses were carried out using R version 3.6.1, including the packages FactoMineR_2.0, factoextra_1.0.6, ggplot2_3.2.1, psych_2.0.7, ARTool_0.10.6, mice_3.13.0, effsize_0.7.6, car_3.0-5, Rmisc_1.5, agricolae_1.3-1, rcompanion_2.3.7, FSA_0.8.26, lattice_0.20-38, plyr_1.8.5, and GraphPad Prism version 8 (La Jolla, CA, USA). Pathway enrichment analyses were performed using Ingenuity Pathway Analysis version 01-18-06 (Ingenuity Systems, Redwood City, CA, USA).

Reporting summary

Further information on research design is available in the Nature Portfolio Reporting Summary linked to this article.

Data availability

Raw phenotypic and molecular data from Figs. 2, 3, 6, 8 were deposited on Mendeley at <https://data.mendeley.com/datasets/ypz9zyc9rp/draft?a=09b16f74-4581-48f7-94af-469e01757949>. The data from the intermittent fasting cohort of mice reused in this study were obtained from one of our previous studies¹⁰ and are accessible on Mendeley at <https://data.mendeley.com/datasets/ypz9zyc9rp/draft?a=09b16f74-4581-48f7-94af-469e01757949>. Raw sequencing data from Fig. 2, Supplementary Figs. 3, 9 are available through GEO datasets at accession number [GSE168068](https://www.ncbi.nlm.nih.gov/geo/query/acc.cgi?acc=GSE168068). The Rhineland Study's dataset is not publicly available because of data protection regulations. Access to data can be provided to scientists in accordance with the Rhineland Study's Data Use and Access Policy. Requests for further information or to access the Rhineland Study's dataset should be directed to RS-DUAC@dz-ne.de. Source data are provided with this paper.

Code availability

Analysis code is available at https://github.com/ehninger/Xie_et_al_longevity_regulators¹³⁷.

References

- Tacutu, R. et al. Human Ageing Genomic Resources: new and updated databases. *Nucleic Acids Res.* **46**, D1083–D1090 (2018).
- Barardo, D. et al. The DrugAge database of aging-related drugs. *Aging Cell* **16**, 594–597 (2017).
- Miller, R.A. Biology of Aging and Longevity. In: *Hazzard's Geriatric Medicine and Gerontology* (eds. Halter, J.B. et al.) (McGraw Hill, 2009).
- Lopez-Otin, C., Blasco, M. A., Partridge, L., Serrano, M. & Kroemer, G. The hallmarks of aging. *Cell* **153**, 1194–1217 (2013).
- Blackwell, B. N., Bucci, T. J., Hart, R. W. & Turturro, A. Longevity, body weight, and neoplasia in ad libitum-fed and diet-restricted C57BL6 mice fed NIH-31 open formula diet. *Toxicol. Pathol.* **23**, 570–582 (1995).
- Pettan-Brewer, C. & Treuting, P. M. Practical pathology of aging mice. *Pathobiol. Aging Age-Relat. Dis.* **1**, 7202 (2011).
- Brayton, C. F., Treuting, P. M. & Ward, J. M. Pathobiology of aging mice and GEM: background strains and experimental design. *Vet. Pathol.* **49**, 85–105 (2012).
- Lipman, R., Galecki, A., Burke, D. T. & Miller, R. A. Genetic loci that influence cause of death in a heterogeneous mouse stock. *J. Gerontol. A Biol. Sci. Med. Sci.* **59**, 977–983 (2004).
- Miller, R. A. et al. Rapamycin, but not resveratrol or simvastatin, extends life span of genetically heterogeneous mice. *J. Gerontol. A Biol. Sci. Med. Sci.* **66**, 191–201 (2011).
- Xie, K. et al. Every-other-day feeding extends lifespan but fails to delay many symptoms of aging in mice. *Nat. Commun.* **8**, 155 (2017).
- Rose, M. R. *Evolutionary biology of aging*, (Oxford University Press, Oxford, 1991).
- Rockstein, M., Chesky, J. A. & Sussman, M. Comparative biology and evolution of aging. In: *Handbook of the biology of aging* 3–34 (Van Nostrand Reinhold Company, New York, 1977).
- Aspinall, R. *Aging of the Organs and Systems*, (Kluwer Academic Publishers, 2003).
- Abdulla, A. & Rai, G.S. *The biology of ageing and its clinical implications*, (Radcliffe Publishing, London, 2013).
- Freund, A. Untangling Aging Using Dynamic, Organism-Level Phenotypic Networks. *Cell Syst.* **8**, 172–181 (2019).
- Neff, F. et al. Rapamycin extends murine lifespan but has limited effects on aging. *J. Clin. Invest.* **123**, 3272–3291 (2013).
- Bellantuono, I. et al. A toolbox for the longitudinal assessment of healthspan in aging mice. *Nat. Protoc.* **15**, 540–574 (2020).
- Ehninger, D., Neff, F. & Xie, K. Longevity, aging and rapamycin. *Cell Mol. Life Sci.* **71**, 4325–4346 (2014).
- Richardson, A. & McCarter, R. Mechanism of food restriction: change of rate or change of set point. In: *The potential for nutritional modulation of aging processes* (eds. Ingram, D. K., Baker, G. T. & Shock, N. W.) 177–192 (Food & Nutrition Press, Inc., 1992).
- Meszaros, L., Hoffmann, A., Wihan, J. & Winkler, J. Current Symptomatic and Disease-Modifying Treatments in Multiple System Atrophy. *Int. J. Mol. Sci.* **21**, 2775 (2020).
- Hampel, H. et al. Biomarkers for Alzheimer's disease: academic, industry and regulatory perspectives. *Nat. Rev. Drug Disco.* **9**, 560–574 (2010).
- Cummings, J. & Fox, N. Defining Disease Modifying Therapy for Alzheimer's Disease. *J. Prev. Alzheimers Dis.* **4**, 109–115 (2017).
- Espay, A. & Stecher, B. Symptomatic vs. Disease-Modifying Therapies. in *Brain Fables: The Hidden History of Neurodegenerative Diseases and a Blueprint to Conquer Them* 87–93 (Cambridge University Press, 2020).
- Vellai, T. et al. Genetics: influence of TOR kinase on lifespan in *C. elegans*. *Nature* **426**, 620 (2003).
- Kapahi, P. et al. Regulation of lifespan in *Drosophila* by modulation of genes in the TOR signaling pathway. *Curr. Biol.* **14**, 885–890 (2004).
- Jia, K., Chen, D. & Riddle, D. L. The TOR pathway interacts with the insulin signaling pathway to regulate *C. elegans* larval development, metabolism and life span. *Development* **131**, 3897–3906 (2004).
- Pan, K. Z. et al. Inhibition of mRNA translation extends lifespan in *Caenorhabditis elegans*. *Aging Cell* **6**, 111–119 (2007).
- Harrison, D. E. et al. Rapamycin fed late in life extends lifespan in genetically heterogeneous mice. *Nature* **460**, 392–395 (2009).
- Chen, C., Liu, Y. & Zheng, P. mTOR regulation and therapeutic rejuvenation of aging hematopoietic stem cells. *Sci. Signal* **2**, ra75 (2009).
- Bjedov, I. et al. Mechanisms of life span extension by rapamycin in the fruit fly *Drosophila melanogaster*. *Cell Metab.* **11**, 35–46 (2010).
- Anisimov, V. N. et al. Rapamycin increases lifespan and inhibits spontaneous tumorigenesis in inbred female mice. *Cell Cycle* **10**, 4230–4236 (2011).
- Robida-Stubbs, S. et al. TOR signaling and rapamycin influence longevity by regulating SKN-1/Nrf and DAF-16/FoxO. *Cell Metab.* **15**, 713–724 (2012).
- Johnson, S. C., Rabinovitch, P. S. & Kaeberlein, M. mTOR is a key modulator of ageing and age-related disease. *Nature* **493**, 338–345 (2013).
- Zhang, Y. et al. Rapamycin Extends Life and Health in C57BL/6 Mice. *J. Gerontol. A Biol. Sci. Med. Sci.* **69**, 119–130 (2014).

35. Wu, J. J. et al. Increased mammalian lifespan and a segmental and tissue-specific slowing of aging after genetic reduction of mTOR expression. *Cell Rep.* **4**, 913–920 (2013).
36. Miller, R. A. et al. Rapamycin-Mediated Lifespan Increase in Mice is Dose and Sex-Dependent and Appears Metabolically Distinct from Dietary Restriction. *Aging Cell* **13**, 468–477 (2014).
37. Fok, W. C. et al. Mice fed rapamycin have an increase in lifespan associated with major changes in the liver transcriptome. *PLoS One* **9**, e83988 (2014).
38. Arriola Apelo, S. I., Pumper, C. P., Baar, E. L., Cummings, N. E. & Lamming, D. W. Intermittent Administration of Rapamycin Extends the Life Span of Female C57BL/6J Mice. *J. Gerontol. A Biol. Sci. Med. Sci.* **71**, 876–881 (2016).
39. Bitto, A. et al. Transient rapamycin treatment can increase lifespan and healthspan in middle-aged mice. *Elife* **5**, e16351 (2016).
40. Wang, T. et al. Epigenetic aging signatures in mice livers are slowed by dwarfism, calorie restriction and rapamycin treatment. *Genome Biol.* **18**, 57 (2017).
41. Schinaman, J. M., Rana, A., Ja, W. W., Clark, R. I. & Walker, D. W. Rapamycin modulates tissue aging and lifespan independently of the gut microbiota in *Drosophila*. *Sci. Rep.* **9**, 7824 (2019).
42. Ferrara-Romeo, I. et al. The mTOR pathway is necessary for survival of mice with short telomeres. *Nat. Commun.* **11**, 1168 (2020).
43. Strong, R. et al. Rapamycin-mediated mouse lifespan extension: Late-life dosage regimes with sex-specific effects. *Aging Cell* **19**, e13269 (2020).
44. Kenyon, C., Chang, J., Gensch, E., Rudner, A. & Tabtiang, R. A *C. elegans* mutant that lives twice as long as wild type. *Nature* **366**, 461–464 (1993).
45. Friedman, D. B. & Johnson, T. E. A mutation in the age-1 gene in *Caenorhabditis elegans* lengthens life and reduces hermaphrodite fertility. *Genetics* **118**, 75–86 (1988).
46. Flurkey, K., Papaconstantinou, J. & Harrison, D. E. The Snell dwarf mutation Pit1(dw) can increase life span in mice. *Mech. Ageing Dev.* **123**, 121–130 (2002).
47. Ikeno, Y., Bronson, R. T., Hubbard, G. B., Lee, S. & Bartke, A. Delayed occurrence of fatal neoplastic diseases in ames dwarf mice: correlation to extended longevity. *J. Gerontol. A Biol. Sci. Med. Sci.* **58**, 291–296 (2003).
48. Ikeno, Y. et al. Reduced incidence and delayed occurrence of fatal neoplastic diseases in growth hormone receptor/binding protein knockout mice. *J. Gerontol. A Biol. Sci. Med. Sci.* **64**, 522–529 (2009).
49. Masternak, M. M., Panici, J. A., Bonkowski, M. S., Hughes, L. F. & Bartke, A. Insulin sensitivity as a key mediator of growth hormone actions on longevity. *J. Gerontol. A Biol. Sci. Med. Sci.* **64**, 516–521 (2009).
50. Sun, L.Y. et al. Longevity is impacted by growth hormone action during early postnatal period. *Elife* **6**, e24059 (2017).
51. Mattison, J. A. et al. Studies of aging in ames dwarf mice: Effects of caloric restriction. *J. Am. Aging Assoc.* **23**, 9–16 (2000).
52. Brown-Borg, H. M. et al. Growth hormone signaling is necessary for lifespan extension by dietary methionine. *Aging Cell* **13**, 1019–1027 (2014).
53. Aguiar-Oliveira, M. H. & Bartke, A. Growth Hormone Deficiency: Health and Longevity. *Endocr. Rev.* **40**, 575–601 (2019).
54. Vitale, G., Pellegrino, G., Vollery, M. & Hofland, L. J. ROLE of IGF-1 System in the Modulation of Longevity: Controversies and New Insights From a Centenarians' Perspective. *Front Endocrinol. (Lausanne)* **10**, 27 (2019).
55. Duran-Ortiz, S. et al. Growth hormone receptor gene disruption in mature-adult mice improves male insulin sensitivity and extends female lifespan. *Aging Cell* **20**, e13506 (2021).
56. Lamming, D. W. Extending Lifespan by Inhibiting the Mechanistic Target of Rapamycin (mTOR). In: *Anti-aging Drugs: From Basic Research to Clinical Practice* (ed. Vaiserman, A.M.) 352–375 (The Royal Society of Chemistry, 2017).
57. Zhang, S. et al. Constitutive reductions in mTOR alter cell size, immune cell development, and antibody production. *Blood* **117**, 1228–1238 (2011).
58. Zhang, S. et al. B cell-specific deficiencies in mTOR limit humoral immune responses. *J. Immunol.* **191**, 1692–1703 (2013).
59. Eicher, E. M. & Beamer, W. G. Inherited ateliotic dwarfism in mice. Characteristics of the mutation, little, on chromosome 6. *J. Hered.* **67**, 87–91 (1976).
60. Flurkey, K., Papaconstantinou, J., Miller, R. A. & Harrison, D. E. Lifespan extension and delayed immune and collagen aging in mutant mice with defects in growth hormone production. *Proc. Natl Acad. Sci. USA* **98**, 6736–6741 (2001).
61. Ward, D. D. et al. Association of retinal layer measurements and adult cognitive function: A population-based study. *Neurology* **95**, e1144–e1152 (2020).
62. McCay, C. M., Crowell, M. F. & Maynard, L. A. The effect of retarded growth upon the length of life span and upon the ultimate body size. *J. Nutr.* **10**, 63–79 (1935).
63. Goodrick, C. L., Ingram, D. K., Reynolds, M. A., Freeman, J. R. & Cider, N. Effects of intermittent feeding upon body weight and lifespan in inbred mice: interaction of genotype and age. *Mech. Ageing Dev.* **55**, 69–87 (1990).
64. Someya, S. et al. Age-related hearing loss in C57BL/6J mice is mediated by Bak-dependent mitochondrial apoptosis. *Proc. Natl Acad. Sci. USA* **106**, 19432–19437 (2009).
65. Henson, S. M. & Aspinall, R. Aging and the Immune System. In: *Aging of Organs and Systems* (ed. Aspinall, R.) 225–242 (Kluwer Academic Publishers, 2003).
66. Linton, P. J. & Dorshkind, K. Age-related changes in lymphocyte development and function. *Nat. Immunol.* **5**, 133–139 (2004).
67. Dorshkind, K., Montecino-Rodriguez, E. & Signer, R. A. The ageing immune system: is it ever too old to become young again? *Nat. Rev. Immunol.* **9**, 57–62 (2009).
68. Bonda, T. A. et al. Remodeling of the intercalated disc related to aging in the mouse heart. *J. Cardiol.* **68**, 261–268 (2016).
69. Mason, J. W. et al. Electrocardiographic reference ranges derived from 79,743 ambulatory subjects. *J. Electrocardiol.* **40**, 228–234 (2007).
70. Wilkinson, J. E. et al. Rapamycin slows aging in mice. *Aging Cell* **11**, 675–682 (2012).
71. Bartke, A. Growth Hormone and Aging: Updated Review. *World J. Mens. Health* **37**, 19–30 (2019).
72. Bartke, A. & Quainoo, N. Impact of Growth Hormone-Related Mutations on Mammalian Aging. *Front Genet* **9**, 586 (2018).
73. Garcia, J. M., Merriam, G. R. & Kargi, A. Y. Growth Hormone in Aging. In: *Endotext* (eds. Feingold, K. R. et al.) (South Dartmouth (MA), 2000).
74. Kim, S. S. & Lee, C. K. Growth signaling and longevity in mouse models. *BMB Rep.* **52**, 70–85 (2019).
75. Carrie, I., Debray, M., Bourre, J. M. & Frances, H. Age-induced cognitive alterations in OF1 mice. *Physiol. Behav.* **66**, 651–656 (1999).
76. GTEx Consortium. The GTEx Consortium atlas of genetic regulatory effects across human tissues. *Science* **369**, 1318–1330 (2020).
77. Shan, T. et al. Adipocyte-specific deletion of mTOR inhibits adipose tissue development and causes insulin resistance in mice. *Diabetologia* **59**, 1995–2004 (2016).
78. Selman, C. Dietary restriction and the pursuit of effective mimetics. *Proc. Nutr. Soc.* **73**, 260–270 (2014).
79. Speakman, J. R. & Mitchell, S. E. Caloric restriction. *Mol. Asp. Med* **32**, 159–221 (2011).

80. Bordner, K. A. et al. Parallel declines in cognition, motivation, and locomotion in aging mice: association with immune gene upregulation in the medial prefrontal cortex. *Exp. Gerontol.* **46**, 643–659 (2011).
81. Sprott, R. L. & Eleftheriou, B. E. Open-field behavior in aging inbred mice. *Gerontologia* **20**, 155–162 (1974).
82. Alderman, J. M. et al. Neuroendocrine inhibition of glucose production and resistance to cancer in dwarf mice. *Exp. Gerontol.* **44**, 26–33 (2009).
83. Keshavarz, M., Xie, K., Schaaf, K., Bano, D. & Ehninger, D. Targeting the “hallmarks of aging” to slow aging and treat age-related disease: fact or fiction? *Mol. Psychiatry* <https://doi.org/10.1038/s41380-022-01680-x> (2022).
84. Blagosklonny, M. V. Validation of anti-aging drugs by treating age-related diseases. *Aging* **1**, 281–288 (2009).
85. Blagosklonny, M. V. Rapamycin and quasi-programmed aging: four years later. *Cell Cycle* **9**, 1859–1862 (2010).
86. Xiang, L. & He, G. Caloric restriction and antiaging effects. *Ann. Nutr. Metab.* **58**, 42–48 (2011).
87. Blagosklonny, M. V. Prospective treatment of age-related diseases by slowing down aging. *Am. J. Pathol.* **181**, 1142–1146 (2012).
88. Sohal, R. S. & Forster, M. J. Caloric restriction and the aging process: a critique. *Free Radic. Biol. Med.* **73**, 366–382 (2014).
89. Blagosklonny, M. V. From rapalogs to anti-aging formula. *Oncotarget* **8**, 35492–35507 (2017).
90. Klimova, B., Novotny, M. & Kuca, K. Anti-Aging Drugs - Prospect of Longer Life? *Curr. Med Chem.* **25**, 1946–1953 (2018).
91. Flanagan, E. W., Most, J., Mey, J. T. & Redman, L. M. Calorie Restriction and Aging in Humans. *Annu Rev. Nutr.* **40**, 105–133 (2020).
92. Mueller, L. D., Rauser, C. L. & Rose, M. R. Aging Stops: Late Life, Evolutionary Biology, and Gerontology. In: *Does Aging Stop?* (Oxford University Press, New York, 2011).
93. Petr, M. A. et al. A cross-sectional study of functional and metabolic changes during aging through the lifespan in male mice. *Elife* **10**, e62952 (2021).
94. Yang, A. C. et al. Physiological blood-brain transport is impaired with age by a shift in transcytosis. *Nature* **583**, 425–430 (2020).
95. Schaum, N. et al. Ageing hallmarks exhibit organ-specific temporal signatures. *Nature* **583**, 596–602 (2020).
96. Tabula Muris, C. A single-cell transcriptomic atlas characterizes ageing tissues in the mouse. *Nature* **583**, 590–595 (2020).
97. Ximerakis, M. et al. Single-cell transcriptomic profiling of the aging mouse brain. *Nat. Neurosci.* **22**, 1696–1708 (2019).
98. Fischer, K. E. et al. A cross-sectional study of male and female C57BL/6Nia mice suggests lifespan and healthspan are not necessarily correlated. *Aging (Albany NY)* **8**, 2370–2391 (2016).
99. Hayflick, L. When does aging begin? *Res Aging* **6**, 99–103 (1984).
100. Papadopoli, D. et al. mTOR as a central regulator of lifespan and aging. *F1000Res.* **8** <https://doi.org/10.12688/f1000research.17196.1> (2019).
101. Martineau, C. N., Brown, A. E. X. & Laurent, P. Multidimensional phenotyping predicts lifespan and quantifies health in *Caenorhabditis elegans*. *PLoS Comput Biol.* **16**, e1008002 (2020).
102. Zhang, W. B. et al. Extended Twilight among Isogenic *C. elegans* Causes a Disproportionate Scaling between Lifespan and Health. *Cell Syst.* **3**, 333–345 e334 (2016).
103. Rockwood, K. & Mitnitski, A. Frailty in relation to the accumulation of deficits. *J. Gerontol. A Biol. Sci. Med. Sci.* **62**, 722–727 (2007).
104. Fried, L. P. et al. Frailty in older adults: evidence for a phenotype. *J. Gerontol. A Biol. Sci. Med. Sci.* **56**, M146–M156 (2001).
105. Bell, C. G. et al. DNA methylation aging clocks: challenges and recommendations. *Genome Biol.* **20**, 249 (2019).
106. Xie, K. et al. Epigenetic alterations in longevity regulators, reduced life span, and exacerbated aging-related pathology in old father offspring mice. *Proc. Natl Acad. Sci. USA* **115**, E2348–E2357 (2018).
107. Franceschi, C. & Campisi, J. Chronic inflammation (inflammaging) and its potential contribution to age-associated diseases. *J. Gerontol. A Biol. Sci. Med. Sci.* **69**(Suppl 1), S4–S9 (2014).
108. Shavlakadze, T. et al. Age-Related Gene Expression Signature in Rats Demonstrate Early, Late, and Linear Transcriptional Changes from Multiple Tissues. *Cell Rep.* **28**, 3263–3273 e3263 (2019).
109. Mair, W., Goymer, P., Pletcher, S. D. & Partridge, L. Demography of dietary restriction and death in *Drosophila*. *Science* **301**, 1731–1733 (2003).
110. Hughes, B. G. & Hekimi, S. Different Mechanisms of Longevity in Long-Lived Mouse and *Caenorhabditis elegans* Mutants Revealed by Statistical Analysis of Mortality Rates. *Genetics* **204**, 905–920 (2016).
111. Hahm, J. H. et al. *C. elegans* maximum velocity correlates with healthspan and is maintained in worms with an insulin receptor mutation. *Nat. Commun.* **6**, 8919 (2015).
112. Zhao, Y. et al. Two forms of death in ageing *Caenorhabditis elegans*. *Nat. Commun.* **8**, 15458 (2017).
113. Podshivalova, K., Kerr, R. A. & Kenyon, C. How a Mutation that Slows Aging Can Also Disproportionately Extend End-of-Life Decrepitude. *Cell Rep.* **19**, 441–450 (2017).
114. Stroustrup, N. et al. The temporal scaling of *Caenorhabditis elegans* ageing. *Nature* **530**, 103–107 (2016).
115. Cohen, A. A., Levasseur, M., Raina, P., Fried, L. P. & Fulop, T. Is Aging Biology Ageist? *J. Gerontol. A Biol. Sci. Med. Sci.* **75**, 1653–1655 (2020).
116. Le Couteur, D. G. & Simpson, S. J. Adaptive senescence: the prolongevity effects of aging. *J. Gerontol. A Biol. Sci. Med. Sci.* **66**, 179–182 (2011).
117. Fuchs, H. et al. Mouse phenotyping. *Methods* **53**, 120–135 (2011).
118. Gailus-Durner, V. et al. Systemic first-line phenotyping. *Methods Mol. Biol.* **530**, 463–509 (2009).
119. Rogers, D. C. et al. Behavioral and functional analysis of mouse phenotype: SHIRPA, a proposed protocol for comprehensive phenotype assessment. *Mamm. Genome* **8**, 711–713 (1997).
120. Jones, B. J. & Roberts, D. J. A rotarod suitable for quantitative measurements of motor incoordination in naive mice. *Naunyn Schmiedebergs Arch. Exp. Pathol. Pharmacol.* **259**, 211 (1968).
121. Schoensiegel, F. et al. High throughput echocardiography in conscious mice: training and primary screens. *Ultraschall Med* **32**(Suppl 1), S124–S129 (2011).
122. Roth, D. M., Swaney, J. S., Dalton, N. D., Gilpin, E. A. & Ross, J. Jr. Impact of anesthesia on cardiac function during echocardiography in mice. *Am. J. Physiol. Heart Circ. Physiol.* **282**, H2134–H2140 (2002).
123. Fischer, M. D. et al. Noninvasive, in vivo assessment of mouse retinal structure using optical coherence tomography. *PLoS One* **4**, e7507 (2009).
124. Schmucker, C. & Schaeffel, F. In vivo biometry in the mouse eye with low coherence interferometry. *Vis. Res.* **44**, 2445–2456 (2004).
125. Prusky, G. T., Alam, N. M., Beekman, S. & Douglas, R. M. Rapid quantification of adult and developing mouse spatial vision using a virtual optomotor system. *Invest Ophthalmol. Vis. Sci.* **45**, 4611–4616 (2004).
126. Rathkolb, B. et al. Blood Collection from Mice and Hematological Analyses on Mouse Blood. *Curr. Protoc. Mouse Biol.* **3**, 101–119 (2013).
127. Weaver, J. L., Broud, D. D., McKinnon, K. & Germolec, D. R. Serial phenotypic analysis of mouse peripheral blood leukocytes. *Toxicol. Mech. Methods* **12**, 95–118 (2002).

128. Roederer, M., Nozzi, J. L. & Nason, M. C. SPICE: exploration and analysis of post-cytometric complex multivariate datasets. *Cytom. A* **79**, 167–174 (2011).
129. Baumgarth, N. & Roederer, M. A practical approach to multicolor flow cytometry for immunophenotyping. *J. Immunol. Methods* **243**, 77–97 (2000).
130. Hou, Z. et al. A cost-effective RNA sequencing protocol for large-scale gene expression studies. *Sci. Rep.* **5**, 9570 (2015).
131. Lawrence, M., Gentleman, R. & Carey, V. rtracklayer: an R package for interfacing with genome browsers. *Bioinformatics* **25**, 1841–1842 (2009).
132. Love, M. I., Huber, W. & Anders, S. Moderated estimation of fold change and dispersion for RNA-seq data with DESeq2. *Genome Biol.* **15**, 550 (2014).
133. Li, Y., Tomko, R. J. Jr. & Hochstrasser, M. Proteasomes: Isolation and Activity Assays. *Curr. Protoc. Cell Biol.* **67**, 3 43 41–43 43 20 (2015).
134. Driver, A. S., Kodavanti, P. R. & Mundy, W. R. Age-related changes in reactive oxygen species production in rat brain homogenates. *Neurotoxicol. Teratol.* **22**, 175–181 (2000).
135. Aziz, N. A. et al. Seroprevalence and correlates of SARS-CoV-2 neutralizing antibodies: Results from a population-based study in Bonn, Germany. *Nat. Commun.* **12**, 2117 (2020).
136. Estrada, S. et al. FatSegNet: A fully automated deep learning pipeline for adipose tissue segmentation on abdominal dixon MRI. *Magn. Reson. Med.* **83**, 1471–1483 (2020).
137. Ehninger, D. Deep Phenotyping and Lifetime Trajectories Reveal Limited Effects of Longevity Regulators on the Aging Process in C57BL/6J Mice. *Zenodo* <https://doi.org/10.5281/zenodo.7142629> (2022).

Acknowledgements

This work was supported by a grant from the Helmholtz Future Topic AMPro (Aging and Metabolic Programming), the German Federal Ministry of Education and Research (Infrafrontier grant O1KX1012), the German Center for Neurodegenerative Diseases (DZNE) and the German Center for Diabetes Research (DZD). Immune phenotyping in the Rhineland Study is partially supported by the Deutsche Forschungsgemeinschaft (DFG, German Research Foundation) under Germany's Excellence Strategy – EXC2151 – 390873048. D.L. was supported by a scholarship from China Scholarship Council. We acknowledge use of the Genotype-Tissue Expression (GTEx) resource supported by the Common Fund of the Office of the Director of the National Institutes of Health, and by NCI, NHGRI, NHLBI, NIDA, NIMH, and NINDS. The data used for the analyses described in this manuscript were obtained from: the GTEx Portal (www.gtexportal.org, accessed on 05/30/20 and 07/15/20). We thank Sach Mukherjee and Gerhard Ehninger for valuable discussions and feedback on an earlier version of the manuscript. We acknowledge Kristian Händler and Joachim L. Schultze for providing access to the PRECISE genomics platform at the DZNE. Figures were created with BioRender.com and/or by adapting from BioRender.com templates.

Author contributions

D.E. conceived and initiated the study; K.X., H.F., V.G.-D. and D.E. planned and prepared the study; K.X., E.S., D.L., A.A., J.A.A.-P., O.V.A., L.B., P.S.-B., J.C.-W., Y.C., Y.D., A.C.E., L.G., C.G., R.G., S.M.H., T.K.-R., D.L., P.M.-K., L.L.N., C.O., B.L.P., B.R., J.Ro., K.S., N.S., A.S.-M., I.T. and D.E. performed the experiments; K.X. E.S., D.L., A.A., J.A.A.-P., O.V.A., L.B., P.S.-B., J.C.-W., Y.C., L.G., R.G., S.M.H., M.K., T.K.-R., D.L., P.M.-K., M.A.O., B.R., J.Ro., J.Ru., N.S., A.S.-M., I.T. and D.E. analyzed the data; K.X., S.L., C.S. and D.E. did project coordination; D.B., D.H.B., J.G., M.K., T.K., B.A.M., P.S., C.S.-W., M.W., E.W., W.W., V.G.-D., M.M.B.B., H.F., M.H.A. and D.E. provided oversight and resources; K.X., E.S., D.L., A.A., B.L.P., D.B. and D.E. wrote the manuscript.

Funding

Open Access funding enabled and organized by Projekt DEAL.

Competing interests

The authors declare no competing interests.

Additional information

Supplementary information The online version contains supplementary material available at <https://doi.org/10.1038/s41467-022-34515-y>.

Correspondence and requests for materials should be addressed to Dan Ehninger.

Peer review information *Nature Communications* thanks Alan Cohen and the other, anonymous, reviewer for their contribution to the peer review of this work.

Reprints and permissions information is available at <http://www.nature.com/reprints>

Publisher's note Springer Nature remains neutral with regard to jurisdictional claims in published maps and institutional affiliations.

Open Access This article is licensed under a Creative Commons Attribution 4.0 International License, which permits use, sharing, adaptation, distribution and reproduction in any medium or format, as long as you give appropriate credit to the original author(s) and the source, provide a link to the Creative Commons license, and indicate if changes were made. The images or other third party material in this article are included in the article's Creative Commons license, unless indicated otherwise in a credit line to the material. If material is not included in the article's Creative Commons license and your intended use is not permitted by statutory regulation or exceeds the permitted use, you will need to obtain permission directly from the copyright holder. To view a copy of this license, visit <http://creativecommons.org/licenses/by/4.0/>.

© The Author(s) 2022

Kan Xie¹, Helmut Fuchs², Enzo Scifo¹, Dan Liu³, Ahmad Aziz^{3,4}, Juan Antonio Aguilar-Pimentel², Oana Veronica Amarie², Lore Becker², Patricia da Silva-Buttkus², Julia Calzada-Wack², Yi-Li Cho², Yushuang Deng¹, A. Cole Edwards¹, Lillian Garrett^{2,5}, Christina Georgopoulou¹, Raffaele Gerlini², Sabine M. Hölder^{2,5}, Tanja Klein-Rodewald², Michael Kramer⁶, Stefanie Leuchtenberger², Dimitra Lountzi¹, Phillip Mayer-Kuckuk², Lena L. Nover¹, Manuela A. Oestereicher², Clemens Overkott¹, Brandon L. Pearson^{1,2,22}, Birgit Rathkolb^{2,7,8}, Jan Rozman^{2,7,23}, Jenny Russ⁹, Kristina Schaa¹, Nadine Spielmann², Adrián Sanz-Moreno², Claudia Stoeger², Irina Treise², Daniele Bano¹⁰, Dirk H. Busch¹¹, Jochen Graw⁵, Martin Klingenspor¹², Thomas Klopstock^{13,14,15}

Beverly A. Mock¹⁶, **Paolo Salomoni**⁹, **Carsten Schmidt-Weber**¹⁷, **Marco Weiergräber**¹⁸, **Eckhard Wolf**⁸, **Wolfgang Wurst**^{5,14,19}, **Valérie Gailus-Durner**², **Monique M. B. Breteler**^{3,20}, **Martin Hrabě de Angelis**^{2,7,21,24} & **Dan Ehninger**^{1,24} ✉

¹Translational Biogerontology Lab, German Center for Neurodegenerative Diseases (DZNE), Venusberg-Campus 1/99, 53127 Bonn, Germany. ²Institute of Experimental Genetics, German Mouse Clinic, Helmholtz Zentrum München, German Research Center for Environmental Health, 85764 Neuherberg, Germany. ³Population Health Sciences, German Center for Neurodegenerative Diseases (DZNE), Venusberg-Campus 1/99, 53127 Bonn, Germany. ⁴Department of Neurology, Faculty of Medicine, University of Bonn, Bonn, Germany. ⁵Institute of Developmental Genetics, Helmholtz Zentrum München, German Research Center for Environmental Health, 85764 Neuherberg, Germany. ⁶GEMoaB GmbH, Tatzberg 47, 01307 Dresden, Germany. ⁷Member of German Center for Diabetes Research (DZD), 85764 Neuherberg, Germany. ⁸Institute of Molecular Animal Breeding and Biotechnology, Gene Center, Ludwig-Maximilians-University Munich, Munich, Germany. ⁹Nuclear Function Lab, German Center for Neurodegenerative Diseases (DZNE), Venusberg-Campus 1/99, 53127 Bonn, Germany. ¹⁰Aging and Neurodegeneration Lab, German Center for Neurodegenerative Diseases (DZNE), Venusberg-Campus 1/99, 53127 Bonn, Germany. ¹¹Institute for Medical Microbiology, Immunology, and Hygiene, Technische Universität München, 81675 Munich, Germany. ¹²Molecular Nutritional Medicine, Else Kröner-Fresenius Center, Technische Universität München, 85350 Freising-Weihenstephan, Germany. ¹³Friedrich-Baur-Institut, Department of Neurology, Ludwig-Maximilians-University Munich, 80336 Munich, Germany. ¹⁴DZNE, German Center for Neurodegenerative Diseases, 80336 Munich, Germany. ¹⁵Munich Cluster for Systems Neurology (SyNergy), 80336 Munich, Germany. ¹⁶Laboratory of Cancer Biology and Genetics, CCR, NCI, NIH, Bethesda, MD 20892, USA. ¹⁷Center of Allergy & Environment (ZAUM), Technische Universität München, and Helmholtz Zentrum München, 85764 Neuherberg, Germany. ¹⁸Research Group Experimental Neuropsychopharmacology, Federal Institute for Drugs and Medical Devices, 53175 Bonn, Germany. ¹⁹Chair of Developmental Genetics, TUM School of Life Sciences (SoLS), Technische Universität München, Freising, Germany. ²⁰Institute for Medical Biometry, Informatics and Epidemiology, Faculty of Medicine, University of Bonn, Venusberg-Campus 1, 53127 Bonn, Germany. ²¹Chair of Experimental Genetics, TUM School of Life Sciences (SoLS), Technische Universität München, 85354 Freising, Germany. ²²Present address: Mailman School of Public Health, Columbia University, 630W. 168th St., New York, NY 10032, USA. ²³Present address: Institute of Molecular Genetics of the Czech Academy of Sciences, Czech Centre for Phenogenomics, Prumyslova 595, Vestec 252 50, Czech Republic. ²⁴These authors contributed equally: Martin Hrabě de Angelis, Dan Ehninger. ✉e-mail: Dan.Ehninger@dzne.de